became undetectable (Fig. 5*B, lane 5*), although its binding capacity to BRCA1-BARD1 was not reduced (data not shown).

To confirm that the many mutations required to make RPB8 resistant to ubiquitination did not impair its fundamental function as a subunit of RNA polymerases, we verified that the 5KR mutant is capable of binding to RPB1 or RPC155 (the largest subunit of polymerase III) *in vivo*. WT FLAG-RPB8 or 5KR was transfected into 293T cells, and anti-FLAG immunocomplexes were isolated. Bound proteins were resolved by SDS-PAGE and analyzed by immunoblotting using anti-RPB1 or anti-RPC155 antibodies. Both RPB1 and RPC155 were detected in the FLAG-5KR immunocomplexes as well as the WT immunocomplexes (Fig. 5*C*). We measured catalytic activity of the anti-FLAG immunoprecipitates using a runoff transcription assay. The 5KR mutant immunocomplexes contained the ability to generate *in vitro* transcripts equal to that of WT immunocomplexes (Fig. 5*D*). Thus, the 5KR mutation of RPB8 constitutes a viable RNA polymerase complex *in vivo* that sustains its polymerase activity. This indicates that RPB8 ubiquitination by BRCA1-BARD1 is not required for RNA polymerase activity.

Ubiquitin-resistant mutant of RPB8 causes UV hypersensitivity. BRCA1 deficiency causes hypersensitivity to DNA damage (14, 26, 27). Because RPB8 is ubiquitinated by BRCA1 after UV irradiation (Fig. 4), it was possible that failure to perform this function could cause the same phenotype. To test this possibility, we established HeLa cell lines that stably express the 5KR mutant of FLAG-RPB8. Two clones each of the WT (WT-1 and WT-2) and of the 5KR (5KR-1 and 5KR-2) cell lines were obtained (Fig. 6*A*). Polyubiquitination of FLAG-RPB8 after UV irradiation was detected in WT cells, but not in mutant cells (Fig. 6*B*). Using these cells, we examined if the expression of the mutant RPB8 affected cell survival after UV irradiation. The cell viabilities of the 5KR clones 48 h after 20 or 35 J/m^2 of UV irradiation were ~38% and 23% of untreated cells at 0 h, respectively, whereas WT clones were ~72% and 53%, respectively (Fig. 6*C*). Parental HeLa cells exhibited viabilities similar to that of WT clones (Fig. 6*C*). Representative data for cells observed by phase contrast microscopy 48 h after UV irradiation (35 J/m^2) and for culture plates stained with Lillie's crystal violet stain are shown (Supplementary Fig. S4). Thus, expression of a ubiquitin-resistant RPB8 form in cells causes UV hypersensitivity.

Because UV-induced cell death is largely ascribable to caspase-induced apoptosis, we next tested whether activation of the caspase pathway by UV irradiation was enhanced in 5KR cells. HeLa cell lines expressing WT or 5KR mutant of FLAG-RPB8 were UV irradiated, and caspase activity was measured by immunoblotting with an antibody to cleaved caspase-3. As shown in Fig. 6*D*, 5KR cells expressed larger amount of cleaved caspase-3 than WT cells did at each time point after UV irradiation. This result suggests that failure to ubiquitinate RPB8 after UV irradiation activates the caspase pathway, resulting in apoptotic cell death.

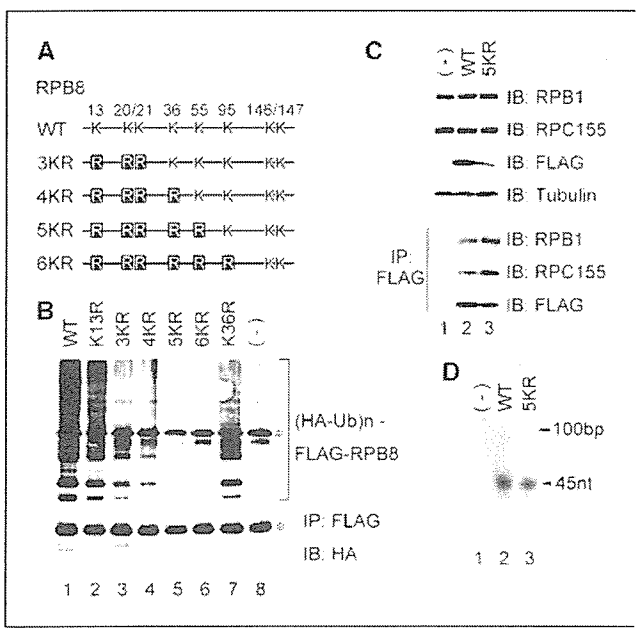

Figure 5. Construction of ubiquitin-resistant RPB8 mutant and assay of its RNA polymerase activity. *A*, the mutant constructs of RPB8. Lys (*K*) residues of RPB8 were substituted with Arg (*R*) as indicated. *B*, Myc-BRCA1$^{1-772}$, BARD1, and HA-ubiquitin were cotransfected into 293T cells either with WT or mutant FLAG-RPB8 as indicated. Polyubiquitination of RPB8 was detected as in Fig. 2*B*. *C*, 293T cells were transfected either with parental pcDNA3 vector (−), WT, or the 5KR mutant of FLAG-RPB8 as indicated. Total cell lysates (*top four panels*) or anti-FLAG immunoprecipitates from equal amounts of total cell lysates (*bottom three panels*) were subjected to immunoblotting with the indicated antibodies. *D*, anti-FLAG immunoprecipitates obtained as in *C* were subjected to an *in vitro* runoff transcription assay using double-stranded DNA templates designed to generate an RNA transcript of 45 nucleotides. Radiolabeled RNA products were resolved by a 12% polyacrylamide/urea gel and scanned with a Typhoon 9400 image analyzer. *, IgG.

Discussion

BRCA1 exists in several different supercomplexes to execute diverse cellular processes. In most of these complexes, BRCA1 exists as a RING heterodimer with BARD1 (28), the form that acquires significant ubiquitin ligase activity (6–8). Revealing the substrates specific for each BRCA1 protein complex is crucial to understand the mechanisms underlying its tumor-suppressor functions.

BRCA1-BARD1 complexes bind to BRCA2 and Rad51 and localize to discrete nuclear foci during S phase. After DNA damage, BRCA1 is phosphorylated by ATM/ATR family kinases (29, 30), and the BRCA1 foci disperse within 30 min (31). The BRCA2-Rad51–containing complex, as well as the BRCA1 complex with Mre11-Rad50-Nbs1, gradually reassemble into different foci (sites of DNA damage) and play important roles in homologous recombination repair. The BRCA1-containing foci begin to appear ~1 h after DNA damage has occurred, reach their peak after 6 to 8 h, and remain until 12 h after damage (31, 32). BRCA1-BARD1 also associates with the RNA polymerase II holoenzyme (15, 16). In contrast to the cases of other complexes described above, BRCA1 dissociates from hyperphosphorylated, processive polymerase II 1 h after DNA damage (17). However, how BRCA1 affects the polymerase II complexes, if at all, during the early stages after DNA damage and before the translocation of BRCA1 to the repair machinery remains to be elucidated. Our results suggest that BRCA1 polyubiquitinates a component of the polymerase II complex, RPB8, at this early stage after DNA damage.

Recently, ubiquitination of phosphorylated RPB1 by BRCA1-BARD1 has been reported (23, 25). Because double knockdown of BRCA1 and BARD1 restored the expression level of the phosphorylated polymerase II that had been repressed by UV irradiation, it was proposed that BRCA1-BARD1 could initiate the degradation of stalled RPB1 (23). However, the BRCA1-BARD1 double knockdown did not detectably affect RPB1 ubiquitination after UV

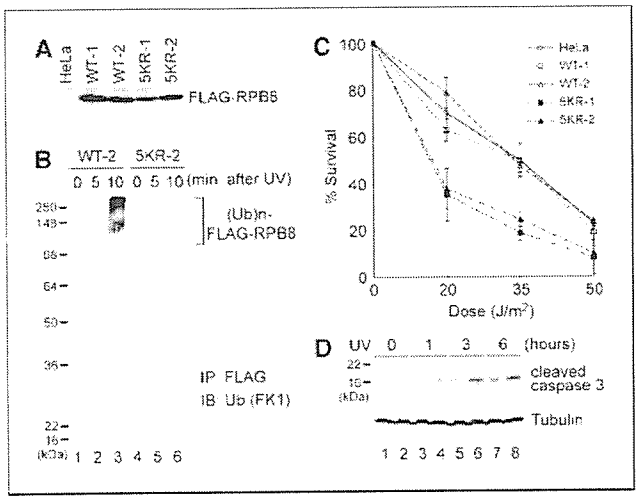

Figure 6. Ubiquitin-resistant RPB8 causes UV hypersensitivity. *A*, cell lysates obtained from two clones each of HeLa cell lines stably expressing either WT (*WT-1* and *WT-2*) or the 5KR mutant (*5KR-1* and *5KR-2*) of FLAG-RPB8 and parental HeLa cells were immunoprecipitated with anti-RPB8 antibody followed by immunoblotting with anti-RPB8 antibody. *B*, HeLa cell lines stably expressing WT (*WT-2, lanes 1–3*) or the 5KR mutant (*5KR-2, lanes 4–6*) of FLAG-RPB8 were UV irradiated (35 J/m^2) and harvested at the indicated times after irradiation. Ubiquitinated RPB8 was detected as described in Fig. 2*B*, except that antipolyubiquitin antibody (*FK1*) was used for immunoblotting. *C*, HeLa cell lines described in *A* were UV irradiated at the indicated doses. Forty-eight hours after irradiation, the cell survival ratio was determined by trypan blue exclusion measurements. The cell number at 0 h (indicated as 0 J/m^2) is 100%. *Points*, mean of measurements carried out in triplicate; *bars*, SD. The experiments were repeated at least twice with similar results. *D*, WT-2 cells (*lanes 1, 3, 5*, and *7*) and 5KR-2 cells (*lanes 2, 4, 6*, and *8*) were UV irradiated (35 J/m^2) and harvested at the indicated times after irradiation. Whole-cell lysates were immunoblotted with anti–caspase-3 antibody or antitubulin antibody.

irradiation. In addition, BRCA1-BARD1–mediated polyubiquitination of other substrates, including NPM1/B23 and phosphorylated CtIP, is not a signal for degradation (12, 33). Therefore, the restored expression level of the phosphorylated polymerase II by BRCA1-BARD1 double knockdown could be due to an indirect effect (23), for example, through the failure to ubiquitinate RPB8. Nonetheless, the clearly shown *in vitro* ubiquitination of phosphorylated RPB1 by BRCA1-BARD1 (23) strongly supports its direct role. The key to solving this discrepancy may be to analyze the timing of RPB1 ubiquitination *in vivo*. RPB1 ubiquitination shown in the previous report occurred 2 h after UV irradiation, when BRCA1 should already be dissociated from polymerase II and relocalized to the Rad50 or Rad51 DNA repair machineries. It is possible that early after DNA damage, RPB1 and RPB8 are transiently ubiquitinated by BRCA1 at the same time, and it may result in dissociation of the polymerase II holoenzyme from the damaged DNA site. RPB1 ubiquitination and degradation occurring in late phases could be mediated by other E3 ligases, such as the CSA-DDB1-CUL4A-ROC1 complex (34, 35).

It is well known that cells with impaired BRCA1 function display hypersensitivity to a range of DNA-damaging agents, including IR and UV irradiation (3, 26). However, the mechanism underlying this phenomenon is not fully understood. Although the failure of checkpoint function is a possible mechanism responsible for the hypersensitivity, it has been reported that neither selective abrogation of the S-phase checkpoint nor the G_2 checkpoint itself results in decreased cell survival after DNA damage (36, 37). Therefore, it has been proposed that some function of BRCA1 other than S-phase or G_2 cell cycle control may affect cell survival after DNA damage (37). The UV hypersensitivity of the cells stably expressing a ubiquitin-resistant mutant of RPB8 shown in this report provides a possible new role for BRCA1 that may compensate for this theoretical defect. Because hyperphosphorylated stalled polymerase II at damaged sites is an extremely cytotoxic ramification of DNA damage (38), the observed UV hypersensitivity could be caused by trapped polymerase II or prolonged polymerase II hyperphosphorylation. In this process, the ubiquitination of RPB8 could be an important step either for polymerase II disassembly, polymerase II dissociation from DNA, or polymerase II dephosphorylation by FCP1. It is interesting that there is considerable expression of endogenous WT RPB8 in the ubiquitin-resistant RPB8 mutant cells (Fig. 4*A*). This indicates that only partial interference of the RNA polymerase recovery is enough to induce cell death, probably by silencing a gene critical for cell survival. Alternatively, polymerase II complexes containing mutant RPB8 could stall at the damaged sites, subsequently causing a gridlock of all polymerase II complexes, including WT complexes. Supporting this idea, induction of local damage by microbeam UV irradiation in the nucleus led to transcription inhibition throughout the nucleus (39).

Lastly, it is noteworthy that RPB8 is shared by all three classes of RNA polymerases (19, 40). Whereas polymerase II synthesizes mRNA, which is only ~5% of all RNAs, polymerase I and polymerase III synthesize the remaining 95% of all RNAs. Therefore, modification of those complexes, rather than polymerase II, might enormously influence cellular conditions. Whereas RPB1 has been intensively studied, the role of RPB8 in the DNA damage response has been poorly understood. The ubiquitination of RPB8 by BRCA1 reported here provides additional evidence for the role of RNA polymerases in the DNA damage response as well as in carcinogenesis.

Acknowledgments

Received 8/31/2006; revised 11/15/2006; accepted 11/30/2006.

Grant support: Japan Society for the Promotion of Science and the Japanese Ministry of Education, Culture, Sports, Science and Technology.

The costs of publication of this article were defrayed in part by the payment of page charges. This article must therefore be hereby marked *advertisement* in accordance with 18 U.S.C. Section 1734 solely to indicate this fact.

We thank Drs. Yanping Zhang, Minoru Takata, and Masamichi Ishiai for helpful discussions and critical reading of the manuscript; and Drs. Richard Baer and Nouria Hernandez for their generous contribution of materials.

References

1. Turner N, Tutt A, Ashworth A. Hallmarks of "BRCA-ness" in sporadic cancers. Nat Rev Cancer 2004;4:814–9.
2. Deng CX. Roles of BRCA1 in centrosome duplication. Oncogene 2002;21:6222–7.
3. Venkitaraman AR. Cancer susceptibility and the functions of BRCA1 and BRCA2. Cell 2002;108:171–82.
4. Zheng L, Li S, Boyer TG, Lee WH. Lessons learned from BRCA1 and BRCA2. Oncogene 2000;19:6159–75.
5. Baer R, Ludwig T. The BRCA1/BARD1 heterodimer, a tumor suppressor complex with ubiquitin E3 ligase activity. Curr Opin Genet Dev 2002;12:86–91.
6. Brzovic PS, Keeffe JR, Nishikawa H, et al. Binding and recognition in the assembly of an active BRCA1/BARD1 ubiquitin-ligase complex. Proc Natl Acad Sci U S A 2003;100:5646–51.
7. Hashizume R, Fukuda M, Maeda I, et al. The RING heterodimer BRCA1-1 is a ubiquitin ligase inactivated by a breast cancer-derived mutation. J Biol Chem 2001;276:14537–40.
8. Mallery DL, Vandenberg CJ, Hiom K. Activation of the E3 ligase function of the BRCA1/BARD1

complex by polyubiquitin chains. EMBO J 2002;21:6755–62.
9. Chau V, Tobias JW, Bachmair A, et al. A multiubiquitin chain is confined to specific lysine in a targeted short-lived protein. Science 1989;243:1576–83.
10. Morris JR, Solomon E. BRCA1: BARD1 induces the formation of conjugated ubiquitin structures, dependent on K6 of ubiquitin, in cells during DNA replication and repair. Hum Mol Genet 2004;13:807–17.
11. Nishikawa H, Ooka S, Sato K, et al. Mass spectrometric and mutational analyses reveal Lys-6-linked polyubiquitin chains catalyzed by BRCA1-1 ubiquitin ligase. J Biol Chem 2004;279:3916–24.
12. Sato K, Hayami R, Wu W, et al. Nucleophosmin/B23 is a candidate substrate for the BRCA1–1 ubiquitin ligase. J Biol Chem 2004;279:30919–22.
13. Wu-Baer F, Lagrazon K, Yuan W, Baer R. The BRCA1/BARD1 heterodimer assembles polyubiquitin chains through an unconventional linkage involving lysine residue K6 of ubiquitin. J Biol Chem 2003;278:34743–6.
14. Ruffner H, Joazeiro CA, Hemmati D, Hunter T, Verma IM. Cancer-predisposing mutations within the RING domain of BRCA1: loss of ubiquitin protein ligase activity and protection from radiation hypersensitivity. Proc Natl Acad Sci U S A 2001;98:5134–9.
15. Chiba N, Parvin JD. The BRCA1 and BARD1 association with the RNA polymerase II holoenzyme. Cancer Res 2002;62:4222–8.
16. Scully R, Anderson SF, Chao DM, et al. BRCA1 is a component of the RNA polymerase II holoenzyme. Proc Natl Acad Sci U S A 1997;94:5605–10.
17. Krum SA, Miranda GA, Lin C, Lane TF. BRCA1 associates with processive RNA polymerase II. J Biol Chem 2003;278:52012–20.
18. Lane TF. BRCA1 and transcription. Cancer Biol Ther 2004;3:528–33.
19. Shpakovski GV, Acker J, Wintzerith M, Lacroix JF, Thuriaux P, Vigneron M. Four subunits that are shared by the three classes of RNA polymerase are functionally interchangeable between *Homo sapiens* and *Saccharomyces cerevisiae*. Mol Cell Biol 1995;15:4702–10.
20. Boulton SJ. BRCA1-mediated ubiquitylation. Cell Cycle 2006;5:1481–6.
21. Kirkpatrick DS, Hathaway NA, Hanna J, et al. Quantitative analysis of *in vitro* ubiquitinated cyclin B1 reveals complex chain topology. Nat Cell Biol 2006;8:700–10.
22. Bregman DB, Halaban R, van Gool AJ, Henning KA, Friedberg EC, Warren SL. UV-induced ubiquitination of RNA polymerase II: a novel modification deficient in Cockayne syndrome cells. Proc Natl Acad Sci U S A 1996;93:11586–90.
23. Kleiman FE, Wu-Baer F, Fonseca D, Kaneko S, Baer R, Manley JL. BRCA1/BARD1 inhibition of mRNA 3′ processing involves targeted degradation of RNA polymerase II. Genes Dev 2005;19:1227–37.
24. Ratner JN, Balasubramanian B, Corden J, Warren SL, Bregman DB. Ultraviolet radiation-induced ubiquitination and proteasomal degradation of the large subunit of RNA polymerase II. Implications for transcription-coupled DNA repair. J Biol Chem 1998;273:5184–9.
25. Starita LM, Horwitz AA, Keogh MC, Ishioka C, Parvin JD, Chiba N. BRCA1/BARD1 ubiquitinate phosphorylated RNA polymerase II. J Biol Chem 2005;280:24498–505.
26. Abbott DW, Thompson ME, Robinson-Benion C, Tomlinson G, Jensen RA, Holt JT. BRCA1 expression restores radiation resistance in BRCA1-defective cancer cells through enhancement of transcription-coupled DNA repair. J Biol Chem 1999;274:18808–12.
27. Shen SX, Weaver Z, Xu X, et al. A targeted disruption of the murine Brca1 gene causes γ-irradiation hypersensitivity and genetic instability. Oncogene 1998;17:3115–24.
28. Greenberg RA, Sobhian B, Pathania S, Cantor SB, Nakatani Y, Livingston DM. Multifactorial contributions to an acute DNA damage response by BRCA1/BARD1-containing complexes. Genes Dev 2006;20:34–46.
29. Cortez D, Wang Y, Qin J, Elledge SJ. Requirement of ATM-dependent phosphorylation of brca1 in the DNA damage response to double-strand breaks. Science 1999;286:1162–6.
30. Tibbetts RS, Cortez D, Brumbaugh KM, et al. Functional interactions between BRCA1 and the checkpoint kinase ATR during genotoxic stress. Genes Dev 2000;14:2989–3002.
31. Scully R, Chen J, Ochs RL, et al. Dynamic changes of BRCA1 subnuclear location and phosphorylation state are initiated by DNA damage. Cell 1997;90:425–35.
32. Zhong Q, Chen CF, Li S, et al. Association of BRCA1 with the hRad50-11-p95 complex and the DNA damage response. Science 1999;285:747–50.
33. Yu X, Fu S, Lai M, Baer R, Chen J. BRCA1 ubiquitinates its phosphorylation-dependent binding partner CtIP. Genes Dev 2006;20:1721–6.
34. Groisman R, Polanowska J, Kuraoka I, et al. The ubiquitin ligase activity in the DDB2 and CSA complexes is differentially regulated by the COP9 signalosome in response to DNA damage. Cell 2003;113:357–67.
35. Hu J, McCall CM, Ohta T, Xiong Y. Targeted ubiquitination of CDT1 by the DDB1–4A-ROC1 ligase in response to DNA damage. Nat Cell Biol 2004;6:1003–9.
36. Xu B, Kim ST, Lim DS, Kastan MB. Two molecularly distinct G(2)/M checkpoints are induced by ionizing irradiation. Mol Cell Biol 2002;22:1049–59.
37. Xu B, O'Donnell AH, Kim ST, Kastan MB. Phosphorylation of serine 1387 in Brca1 is specifically required for the Atm-mediated S-phase checkpoint after ionizing irradiation. Cancer Res 2002;62:4588–91.
38. van den Boom V, Jaspers NG, Vermeulen W. When machines get stuck-obstructed RNA polymerase II: displacement, degradation or suicide. Bioessays 2002;24:780–4.
39. Takeda S, Naruse S, Yatani R. Effects of ultra-violet microbeam irradiation of various sites of HeLa cells on the synthesis of RNA, DNA and protein. Nature 1967;213:696–7.
40. Briand JF, Navarro F, Rematier P, et al. Partners of Rpb8p, a small subunit shared by yeast RNA polymerases I, II and III. Mol Cell Biol 2001;21:6056–65.

Regulatory Roles of NKT Cells in the Induction and Maintenance of Cyclophosphamide-Induced Tolerance[1]

Toshiro Iwai,* Yukihiro Tomita,[2]* Shinji Okano,† Ichiro Shimizu,* Yohichi Yasunami,‡ Takashi Kajiwara,* Yasunobu Yoshikai,§ Masaru Taniguchi,‖ Kikuo Nomoto,¶ and Hisataka Yasui*

We have previously reported the sequential mechanisms of cyclophosphamide (CP)-induced tolerance. Permanent acceptance of donor skin graft is readily induced in the MHC-matched and minor Ag-mismatched recipients after treatment with donor spleen cells and CP. In the present study, we have elucidated the roles of NKT cells in CP-induced skin allograft tolerance. BALB/c AnNCrj (H-2^d, Lyt-1.2, and Mls-1^b) wild-type (WT) mice or Vα14 NKT knockout (KO) (BALB/c) mice were used as recipients, and DBA/2 NCrj (H-2^d, Lyt-1.1, and Mls-1^a) mice were used as donors. Recipient mice were primed with 1 × 10^8 donor SC i.v. on day 0, followed by 200 mg/kg CP i.p. on day 2. Donor mixed chimerism and permanent acceptance of donor skin allografts were observed in the WT recipients. However, donor skin allografts were rejected in NKT KO recipient mice. In addition, the donor reactive Vβ6$^+$ T cells were observed in the thymus of a NKT KO recipient. Reconstruction of NKT cells from WT mice restored the acceptance of donor skin allografts. In addition, donor grafts were partially accepted in the thymectomized NKT KO recipient mice. Furthermore, the tolerogen-specific suppressor cell was observed in thymectomized NKT KO recipient mice, suggesting the generation of regulatory T cells in the absence of NTK cells. Our results suggest that NKT cells are essential for CP-induced tolerance and may have a role in the establishment of mixed chimerism, resulting in clonal deletion of donor-reactive T cells in the recipient thymus. *The Journal of Immunology,* **2006, 177: 8400–8409.**

Natural killer T cells, which are characterized by coexpression of NK cell receptors and a single invariant T cell Ag receptor encoded by *Vα14* and *Jα281* gene segments, have been identified as a novel lymphoid lineage distinct from conventional T cells or NK cells. Although the physiological roles of NKT cells remain obscure, Vα14 NKT cells have been demonstrated to play important roles in tumor immunity (1), autoimmune disease (2), and infectious immunity (3, 4) via the dominant production of Th1 cytokine γ-IFN and Th2 cytokine IL-4. Regarding transplantation immunity, two reports have suggested a regulatory role of NKT cells in both allogeneic and xenogeneic tolerance systems induced by mAbs (5, 6).

Since 1982, we have investigated cyclophosphamide (CP)[3]-induced tolerance that consists of an i.v. injection of 1 × 10^8 allogeneic spleen cells (SC) (day 0) followed by i.p. administration of 200 mg/kg CP on day 2 (7–18). By using this method, we were able to readily induce long-lasting skin allograft tolerance in most H-2-matched combinations (10–12), but not in fully H-2-mismatched combinations (7, 13). Our previous studies have elucidated the three major mechanisms involved using H-2-compatible, Mls-1^a-disparate combinations and Mls-1^a Ag-reactive Vβ6$^+$ T cells (11–14). The first is the destruction of Ag-stimulated and then proliferating T cells in the periphery by CP treatment. CD4$^+$Vβ6$^+$ T cells proliferated and then disappeared in the periphery of the recipients tolerized to H-2-compatible, Mls-1^a-disparate Ags. The second, at 4–6 wk after the treatments, is the establishment of intrathymic chimerism at both the thymocyte and dendritic cell levels, followed by the clonal deletion of Vβ6$^+$ T cells that begins in the thymus. The third mechanism is the generation of regulatory cells in the late stage of tolerance.

The aim of the present study was to investigate the regulatory role of NKT cells in our CP-induced tolerance system by using Vα14 NKT knockout (KO) mice. Although an essential role for NKT cells in the induction of transplantation tolerance has been suggested in two previous reports (5, 6), the detailed mechanisms have not been clarified. Here, we evaluated the role of NKT cells in our three important mechanisms, i.e., clonal destruction, intrathymic clonal deletion, and generation of regulatory cells. The results clearly showed that NKT cells were essential for CP-induced tolerance through the establishment of intrathymic clonal deletion. Without NKT cell-mediated immunoregulation, however, our results demonstrated that the generation of regulatory cells for the maintenance of tolerance in the late stage of tolerance can occur, in addition to clonal destruction at the early stage.

Materials and Methods

Animals

Inbred mice of the BALB/c AnNCrj (H-2^d, Lyt-1.2, and Mls-1^b) and DBA/2 NCrj (H-2^d, Lyt-1.1, and Mls-1^a) strains were obtained from

*Department of Cardiovascular Surgery and †Division of Pathophysiological and Experimental Pathology, Department of Pathology, Graduate School of Medical Sciencies, Kyushu University, Fukuoka, Japan; ‡Department of Surgery I, Fukuoka University School of Medicine, Fukuoka, Japan; §Department of Infection Control and ¶Department of Immunology, Medical Institute of Bioregulation, Kyushu University, Fukuoka, Japan; and ‖Laboratory for Immune Regulation, RIKEN Research Center for Allergy and Immunology, Yokohama, Japan

Received for publication March 18, 2004. Accepted for publication September 22, 2006.

The costs of publication of this article were defrayed in part by the payment of page charges. This article must therefore be hereby marked *advertisement* in accordance with 18 U.S.C. Section 1734 solely to indicate this fact.

[1] This study was supported by a Grant-in-Aid for Scientific Research from the Ministry of Health and Welfare, Japan (to Y.T.). Y.T. was also the recipient of a Surgical Research Foundation Grant from the Japanese Surgical Association.

[2] Address correspondence and reprint requests to Dr. Yukihiro Tomita, Department of Cardiovascular Surgery, Graduate School of Medical Sciences, Kyushu University, 3-1-1 Maidashi, Higashi-ku, Fukuoka 812-8582, Japan. E-mail address: tomita@heart.med.kyushu-u.ac.jp

[3] Abbreviations used in this paper: CP, cyclophosphamide; αGalCer, α-galactosyl ceramide; BMC, bone marrow cell; Gy, gray; KO, knockout; LMNC, liver mononuclear cell; MST, mean survival time; SC, spleen cell; WBC, white blood cell; WT, wild type.

0022-1767/06/$02.00

Charles River Laboratories. Inbred mice of the B10.D2 SnSlc (H-2^d) strain were obtained from Japan SLC. Jα281 KO (Vα14 NKT KO) mice with a BALB/c background were also used as recipients (1). The recipients were used at 12–16 wk of age. All animals received humane care in compliance with the Guidelines for Animal Experiments of Kyushu University and Law no. 105 and Notification no. 6 of the Japanese government.

Cell preparation

Mice were sacrificed by decapitation. The spleens were collected and kept on ice in RPMI 1640 medium (Invitrogen Life Technologies) supplemented with antibiotics (100 μg/ml penicillin and 100 μg/ml streptomycin). Spleens were disrupted in the medium by pressing spleen fragments between two glass slides. Cell suspensions were filtered through cotton gauze and washed three times with the RPMI 1640 medium. Viable nucleated cells were counted and usually adjusted to 20×10^7/ml.

Conditioning of CP-induced tolerance

A 0.5-ml aliquot containing 1×10^8 SC from DBA/2 mice was injected into the tail vein of recipient BALB/c mice. Two days later, CP (Endoxan; Shionogi) dissolved in PBS at a concentration of 10 mg/ml was injected i.p. at a dose of 200 mg/kg. The day of the injection of DBA/2 SC is referred to as day 0 throughout this report.

Reconstitution of NKT cells in NKT KO mice

We set up two methods to reconstitute NKT cells in NKT KO mice. First, a 0.5-ml aliquot containing 1×10^8 SC from WT mice (containing ~1% NKT cells) was injected into the tail vein of recipient NKT KO mice on day −7. Second, recipient NKT KO mice were irradiated with three gray (Gy) on day −28 and then reconstituted with 1×10^7 SC and 5×10^6 untreated bone marrow cells (BMC) (containing ~0.1–0.4% NKT cells) from WT mice on the same day. The preparation of BMC was performed according to a previous method (19). Briefly, the bone marrow in the femoral and tibial bones was flushed out using a 5-ml syringe with a 26-gauge needle (Terumo).

Skin grafting

Skin grafting was performed using our previously reported procedure (20). Briefly, a square, full-thickness skin graft (1 cm^2) was prepared on the right lateral thoracic wall of the recipient mouse. The graft was fixed to the graft bed with eight interrupted sutures of 5-0 silk thread and covered with protective tape. The first inspection was conducted on the 7th day, followed by daily inspection for 3 wk. Grafts were considered as rejected at the time of complete sloughing or when they formed a dry scar. Survival was expressed as the median survival time and the mean survival time (MST) ± SD.

Thymectomy

Recipients were anesthetized with phenobarbital (Nembutal) at 50 mg/kg administered i.p. After a partial sternotomy, the thymectomy was performed by en bloc excision using two pairs of forceps (21). The absence of thymic tissue was always confirmed when the thymectomized animals were sacrificed, and animals showing the presence of residual thymic tissue were excluded from the analysis.

Flow cytometry

Phenotyping was performed at various times, beginning 2 wk after the injection of SC. Recipients were tail bled and white blood cells (WBC) were prepared by hypotonic shock (21). In some experiments, SC and thymocytes were used for chimeric assays. Staining with both donor-specific and T cell-specific mAbs was performed on each recipient and control mouse. Cells were incubated with a PE-conjugated anti-Lyt-1 (Lyt-1.1 and Lyt-1.2) (BD Pharmingen) mAb and a FITC-conjugated Lyt-1.1 (BD Pharmingen) mAb for 30 min at 4°C and then washed twice. To block nonspecific FcγR binding of labeled Abs, 10 μl of an undiluted culture supernatant of 2.4G2 (rat anti-mouse FcγR mAb) was used. All data were analyzed with a FACScan (BD Biosciences). Dead cells were excluded by gating out low forward scatter, high propidium iodide-retaining cells.

For the analysis of TCR expression on T cells of SC or WBC, two-color analysis was performed (21). WBC or SC were labeled with FITC-conjugated anti-Vβ6 or Vβ8.1/8.2 mAb (BD Pharmingen), and PE-conjugated anti-CD4 (BD Pharmingen) mAb. To determine the percentage of $CD4^+$ T cells that were $V\beta6^+$ or $V\beta8.1/8.2^+$, 10,000–20,000 gated $CD4^+$ cells were collected. For the analysis of TCR expression on thymocytes, three-color analysis was performed (21). Thymocytes were labeled with FITC-conjugated anti-Vβ6 or Vβ8.1/8.2 mAb (BD Pharmingen), PE-conjugated anti-CD4 (BD Pharmingen) mAb, and allophycocyanin-conjugated anti-CD8 (BD Pharmingen) mAb for 30 min at 4°C. To determine the percentage of CD4 single-positive cells that were $V\beta6^+$ or $V\beta8.1/8.2^+$, 5,000 to 10,000 gated $CD4^+$ and $CD8^-$ cells were collected. We investigated the effect of SC/CP on the ratio of $CD4^+V\beta6^+$ T cell or $CD4^+V\beta8^+$ T cell subsets to the total $CD4^+$ T cell number in the spleen or WBC and on the ratio of $CD4^+CD8^-V\beta6^+$ T cell or $CD4^+CD8^-V\beta8^+$ T cell subsets to the total $CD4^+CD8^-$ T cell number in the thymus. We also investigated the effect of SC/CP on the absolute number of $CD4^+V\beta6^+$ T cells or $CD4^+V\beta8^+$ T cells in the spleen and thymus.

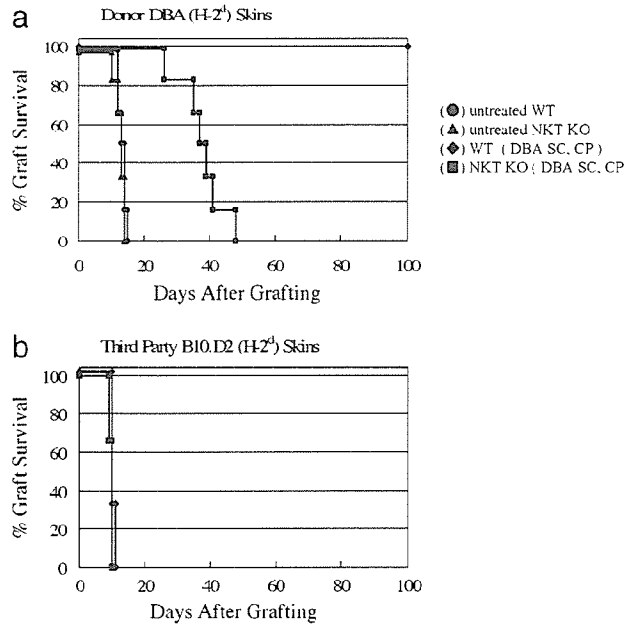

FIGURE 1. Skin allograft survival in the recipient BALB/c mice treated with DBA/2 SC. Recipient mice were grafted with skin from donor DBA/2 (DBA) (*a*) or third party B10.D2 (*b*) mice 4 wk after treatment. *a*, The groups and median skin graft survival times were as follows: ●, Untreated WT mice (n = 6; 13.5 days); ▲, untreated NKT KO mice (n = 6; 13 days); ◆, WT mice treated with DBA/2 SC and CP (n = 6; >100 days); and ■, NKT KO mice treated with DBA/2 SC and CP (n = 6; 38 days). *b*, B10.D2 skin grafts were rejected within 14 days after grafting in the following groups: ◆, WT mice treated with DBA/2 SC and CP (n = 3); ■, NKT KO mice treated with DBA/2 SC and CP (n = 3).

For the staining of NKT cells, SC or liver mononuclear cells (LMNC) were stained with PE-conjugated α-galactosyl ceramide (αGalCer)/CD1d tetramers and FITC-conjugated anti-CD3 mAb (BD Pharmingen). PE-conjugated αGalCer/CD1d tetramers were prepared as previously described (22). The liver was disrupted in RPMI 1640 medium (Invitrogen Life Technologies) supplemented with 10% FCS by pressing liver fragments between two glass slides and then washed, resuspended in a 40% isotonic Percoll solution (Amersham Biosciences) and underlaid with a 67.5% isotonic Percoll solution. Centrifugation for 30 min at 3 000 rpm at room temperature isolated the LMNC at the interface. Cells were washed two times with HBSS containing 2% FCS and resuspended in the same solution.

Adoptive transfer experiment

To elucidate the existence of regulatory cells in the tolerant recipients, adoptive transfer experiments were performed as described previously (14). Briefly, 1×10^8 or 4×10^7 SC from the recipient mice accepting DBA/2 skin allografts for over 100 days were transferred into WT mice that had been irradiated with 3 Gy on the same day. The SC were harvested from WT or NKT mice that had been thymectomized and treated with DBA/2 SC and CP. Skin grafting was performed 1 day following the adoptive transfer. In one experiment, $CD4^+CD8^+Thy1.2^+$ T cell depletion was performed using anti-CD4 mAb (L3/T4), anti-CD8 mAb (Ly2.2) (Cedarlane Laboratories), anti-Thy-1.2 mAb (Meiji), and complement (Low-Tox-M rabbit complement; Cedarlane Laboratories).

Table I. *Chimerism and clonal destruction in WBC of recipients treated with DBA/2 SC and CP*[a]

Group	Recipient	Treatment[a] SC (day 0)	Treatment[a] CP (day 2)	No. of Mice	Chimeric Analysis (percent positive cells ± SD) Lyt-1.1$^+$/Lyt-1$^+$ (%) 2 wk	Lyt-1.1$^+$/Lyt-1$^+$ (%) 8 wk	Analysis of TCR Expression (percent positive cells ± SD) CD4$^+$Vβ6$^+$/CD4$^+$ (%) 3 wk	CD4$^+$Vβ6$^+$/CD4$^+$ (%) 9 wk	CD4$^+$Vβ6$^+$/CD4$^+$ (%) 3 wk	CD4$^+$Vβ6$^+$/CD4$^+$ (%) 9 wk
1	BALB/c WT	(−)	(−)	6	0		10.7 ± 1.2		16.6 ± 1.6	
2	BALB/c NKT KO	(−)	(−)	6	0		11.3 ± 1.4		12.2 ± 1.7	
3	DBA/2	(−)	(−)	6	96.3 ± 2.4		0		13.0 ± 1.1	
4	BALB/c WT	DBA/2	200[b]	6	2.6 ± 0.8[c]	3.8 ± 1.0[c]	1.6 ± 0.5	1.1 ± 0.4	17.1 ± 1.9	16.6 ± 2.0
5	BALB/c NKT KO	DBA/2	200[b]	6	1.5 ± 0.1	0.9 ± 0.2	1.3 ± 0.3	0.8 ± 0.2	12.9 ± 1.2	2.6 ± 1.7

[a] The recipient mice were primed i.v. with 1×10^8 viable DBA/2 SC on day 0 and then given 200 mg/kg CP on day 2.
[b] Milligrams per kilogram (mg/kg).
[c] $p < 0.01$ compared with group 5.

Statistics

The statistical significance of the data was determined by a Mann-Whitney *U* test when the data were nonparametric or a Student's *t* test when the data were parametric. A value of $p < 0.05$ was considered to be statistically significant.

Results

Skin allograft prolongation in H-2-matched DBA/2 (H-2^d) → BALB/c WT (H-2^d) or BALB/c background Vα14 NKT KO (H-2^d) combination mice by using 1×10^8 DBA/2 SC followed by 200 mg/kg CP

When BALB/c WT (H-2^d) or BALB/c background NKT KO mice were grafted with H-2-matched DBA/2 skin allografts (H-2^d), the DBA/2 grafts were rejected within 14 days following grafting (Fig. 1*a*). Similarly, DBA/2 skin grafts were rejected within 14 days in BALB/c WT or NKT KO mice treated with DBA/2 SC alone or 200 mg/kg CP alone (data not shown). All of the DBA/2 skin allografts survived for >100 days in the recipient BALB/c WT mice treated with DBA/2 SC followed by CP ($n = 6$; MST, >100 days). When syngeneic (BALB/c) WT SC or PBS (0.5 ml) was used instead of DBA/2 SC or CP, respectively, the survival times of DBA/2 skin grafts were not prolonged (data not shown). In contrast, all DBA/2 skin grafts were rejected within 48 days in the recipient NKT KO mice treated with DBA/2 SC followed by CP ($n = 6$; MST, 38 days), although the survival of the grafts was moderately prolonged. The skin allograft prolongation in both BALB/c WT mice and NKT KO mice, which were treated with DBA/2 SC followed by CP, was tolerogen-specific, because the third party skin grafts of the B10.D2 strain (H-2^d) were rejected in a normal fashion (Fig. 1*b*).

Chimerism and reduction of Mls-1^a-reactive CD4$^+$Vβ6$^+$ T cells of WBC in the recipient mice treated with DBA/2 SC plus CP

As we previously reported (14), a minimal degree of mixed chimerism was detected in the BALB/c WT (Lyt-1.2) mice made tolerant of DBA/2 (Lyt-1.1) skin allografts. The mixed chimeric state induced with DBA/2 SC and CP was examined using

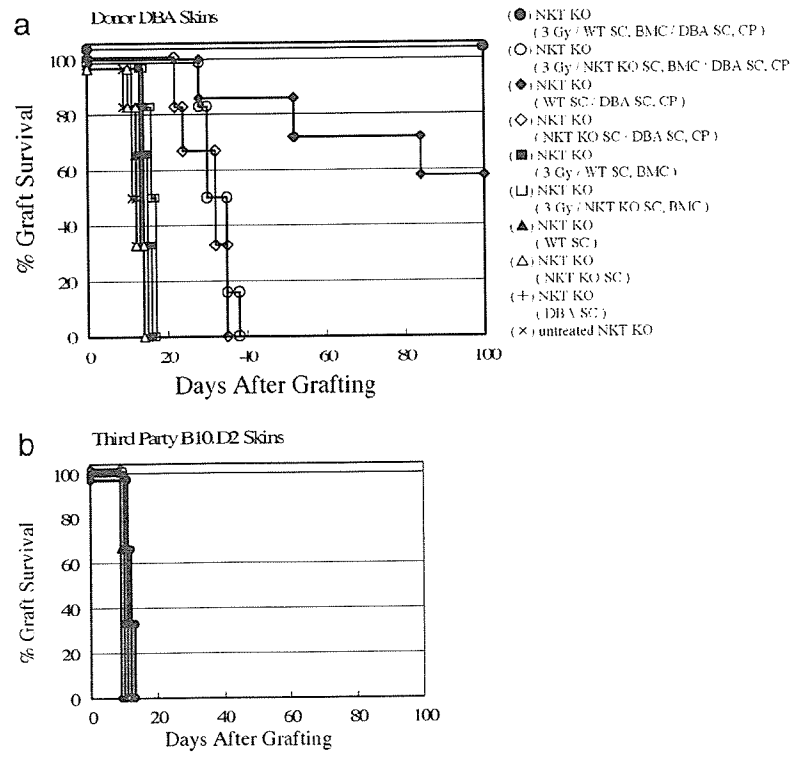

FIGURE 2. Skin allograft survival in recipient BALB/c NKT KO mice reconstituted with NKT cells and treated with DBA/2 SC and CP. Recipient mice were grafted with skin from donor DBA/2 (DBA) (*a*) or third party B10.D2 (*b*) mice 4 wk after treatment. *a* The groups and median skin graft survival times were as follows: ●, NKT KO mice irradiated with 3 Gy followed by reconstitution with WT SC and BMC and treatment with DBA/2 SC and CP ($n = 6$; >100 days); ○, NKT KO mice irradiated with 3 Gy followed by reconstitution with NKT KO SC and BMC and treatment with DBA/2 SC and CP ($n = 6$; 32.5 days); ◆, NKT KO mice reconstituted with WT SC and treated with DBA/2 SC and CP ($n = 7$; >100 days); ◇, NKT KO mice reconstituted with NKT KO SC and treated with DBA/2 SC and CP ($n = 6$; 32 days); ■, NKT KO mice irradiated with 3 Gy followed by reconstitution with WT SC and BMC ($n = 6$; 15 days); □, NKT KO mice irradiated with 3 Gy followed by reconstitution with NKT KO SC and BMC ($n = 6$; 16.5 days); ▲, NKT KO mice reconstituted with WT SC ($n = 6$; 13 days); △, NKT KO mice reconstituted with NKT KO SC ($n = 6$; 12 days); +, NKT KO mice treated with DBA/2 SC alone ($n = 6$; 14 days); and ×, untreated NKT KO mice ($n = 6$; 11.5 days). *b*, B10.BR skin grafts were rejected within 14 days after grafting in all of the groups described above in *a* ($n = 3$ in each group).

PE-conjugated anti-Lyt-1 (Lyt-1.1 and Lyt-1.2) mAb and FITC-conjugated Lyt-1.1 mAb. WBC were obtained from the recipient mice at 2 and 8 wk after tolerance induction (Table I).

In the T (Lyt-1$^+$) cells of BALB/c WT mice treated with DBA/2 SC and CP (Table I; group 4), 2–4% of Lyt-1.1 cells were clearly detected in the recipient WBC after tolerance induction. In contrast, a lower degree of chimerism was clearly detected at 2 wk (mean ± SD, 1.5 ± 0.1; $p < 0.01$ compared with group 4) and became <1% at 8 wk in the T (Lyt-1$^+$) cells of NKT KO mice treated with DBA/2 SC followed by CP (Table I; group 5). A higher degree of chimerism was always observed in recipient BALB/c WT mice treated with DBA/2 SC and CP. These results were reproducible in five independent experiments (data not shown).

We examined the expression of the Mls-1^a-reactive TCR Vβ6 in BALB/c WT or NKT KO (Mls-1^b) mice treated with DBA/2 (Mls-1^a) SC and CP. The WBC from the recipients were stained with FITC-conjugated anti-Vβ6 mAb and PE-conjugated anti-CD4 mAb (Table I).

In the WBC of untreated BALB/c WT or NKT KO mice, CD4$^+$Vβ6$^+$ T cells were detected (Table I; group 1 or 2, respectively), whereas they were hardly detected in the WBC of untreated DBA/2 mice (Table I; group 3). In all of the BALB/c WT mice treated with DBA/2 SC and CP (Table I; group 4), CD4$^+$Vβ6$^+$ T cells were significantly reduced by 3 wk. The same results were obtained in the WBC of NKT KO mice treated with DBA/2 SC and CP (Table I; group 5). There was no statistically significant difference in the results between groups 4 and 5. The disappearance of T cells from the WBC was specific for Vβ6$^+$ T cells, because the percentage of Vβ8.1/8.2$^+$ T cells was not significantly altered.

Induction of DBA/2 skin graft prolongation in NKT KO mice reconstituted with NKT cells from BALB/c WT mice

To clarify whether NKT cells were involved in the limitation of skin graft tolerance in CP-induced tolerance, NKT cells were reconstituted in NKT KO mice (Fig. 2). When SC and LMNC were stained with PE-conjugated αGalCer/CD1d tetramers and FITC-conjugated anti-CD3 mAb, αGalCer/CD1d tetramer$^+$CD3$^+$ cells accounted for ~1.0 ± 0.3 and 19.5 ± 5.4% of SC and LMNC in untreated BALB/c WT mice (n = 3), respectively, and 0.3 ± 0.1 and 1.2 ± 0.2% of SC and LMNC in untreated NKT KO mice (n = 3), respectively. A small percentage of αGalCer/CD1d tetramer$^+$CD3$^+$ cells were detected in NKT KO mice, because the NKT KO mice used in this study were generated by disruption of the *Jα281* gene (1). In contrast, αGalCer/CD1d tetramer$^+$CD3$^+$ cells accounted for ~0.4 ± 0.1 and 4.3 ± 0.5% in SC and LMNC of NKT KO mice (n = 3) injected with BALB/c WT SC 7 days earlier, respectively. Therefore, we planned an additional experiment to further reconstitute NKT cells in NKT KO mice. For this purpose, recipient NKT KO mice were irradiated with 3 Gy on day −28 and then injected with 1 × 10^7 SC and 5 × 10^6 untreated BMC from WT mice on the same day. In NKT KO mice (n = 5) irradiated and injected with BALB/c WT SC and BMC 28 days earlier, αGalCer/CD1d tetramer$^+$CD3$^+$ cells accounted for ~0.7 ± 0.1 and 9.5 ± 2.6% of SC and LMNC, respectively. When NKT KO mice were injected with 1 × 10^8 SC from BALB/c WT mice on day −7 and treated with SC on day 0 and CP on day 2, the survival of DBA/2 skin grafts was significantly prolonged (n = 7; MST, >100 days), and four of seven recipients accepted donor DBA/2 skin grafts for >100 days (Fig. 2*a*). DBA/2 skin grafts were accepted for >100 days in all of the NKT KO mice irradiated with 3 Gy on day −28, reconstituted with 1 × 10^7 SC and 5 × 10^6 BMC from BALB/c WT mice on day −28, and then treated with DBA/2 SC on day 0 and CP on day 2 (Fig. 2*a*). Survival of donor skin grafts was not significantly prolonged in NKT KO mice reconstituted with SC and/or BMC from NKT KO mice and treated with DBA/2 SC and CP as compared with that for NKT KO mice treated with DBA/2 SC and CP. In contrast, no skin graft prolongation was observed in NKT KO mice reconstituted with BALB/c WT SC or BMC, irradiated NKT KO mice reconstituted with BALB/c WT SC and BMC, NKT KO mice reconstituted with NKT KO SC or BMC, or irradiated NKT KO mice reconstituted with NKT SC and BMC if the recipient mice were not treated with donor SC and CP (Fig. 2*a*). This skin allograft prolongation was tolerogen-specific, because the third party skin of the B10.D2 strain (H-2^d) was rejected in a normal fashion (Fig. 2*b*).

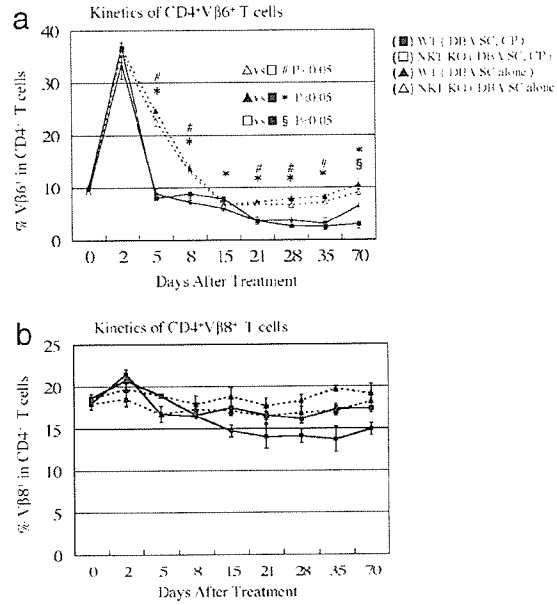

FIGURE 3. Clonal destruction in the periphery of recipient mice. The kinetics of CD4$^+$Vβ6$^+$ (*a*) or CD4$^+$Vβ8.1/8.2$^+$ (*b*) T cells in spleen cells harvested from the recipient mice are shown. SC were labeled with FITC-conjugated anti-Vβ6 or Vβ8.1/8.2 mAb and PE-conjugated anti-CD4 mAb. To determine the percentage of CD4$^+$ T cells that were Vβ6$^+$ or Vβ8.1/8.2$^+$, 10,000–20,000 gated CD4$^+$ cells were collected. SC cells were obtained from WT (H-2^d; Mls-1^b) mice treated with DBA/2 (DBA) (H-2^d; Mls-1^a) SC and CP (■; n = 4), NKT KO mice treated with DBA/2 SC and CP (□; n = 4), WT mice treated with DBA/2 SC alone (▲; n = 4), and NKT KO mice treated with DBA/2 SC alone (△; n = 4). Vertical bars represent the SD. The statistical significance of the differences among groups was analyzed and the results are given in *a*.

Analysis of splenic clonal destruction and intrathymic clonal deletion and mixed chimerism in BALB/c WT or NKT KO mice treated with DBA/2 SC and CP

As reported previously (12, 13), the induction mechanism of CP-induced tolerance is the clonal destruction of Ag-stimulated and proliferating T cells by the antimitotic drug CP. To further analyze the role of NKT cells in the tolerance induction, we examined the kinetics of Mls-1^a-reactive CD4$^+$Vβ6$^+$ T cells in the CD4$^+$ T cells of SC in recipient BALB/c WT or NKT KO mice. When DBA/2 SC were injected into untreated BALB/c WT mice on day 0, CD4$^+$Vβ6$^+$ T cells significantly increased to ~35% on day 2 and then eventually declined to the normal range by days 15–21 (Fig. 3*a*). The same result was observed in NKT KO mice. In BALB/c WT mice treated with DBA/2 SC on day 0 and CP on day 2, CD4$^+$Vβ6$^+$ T cells significantly increased to ~35% on day 2, rapidly decreased to the normal range on day 5, and then gradually

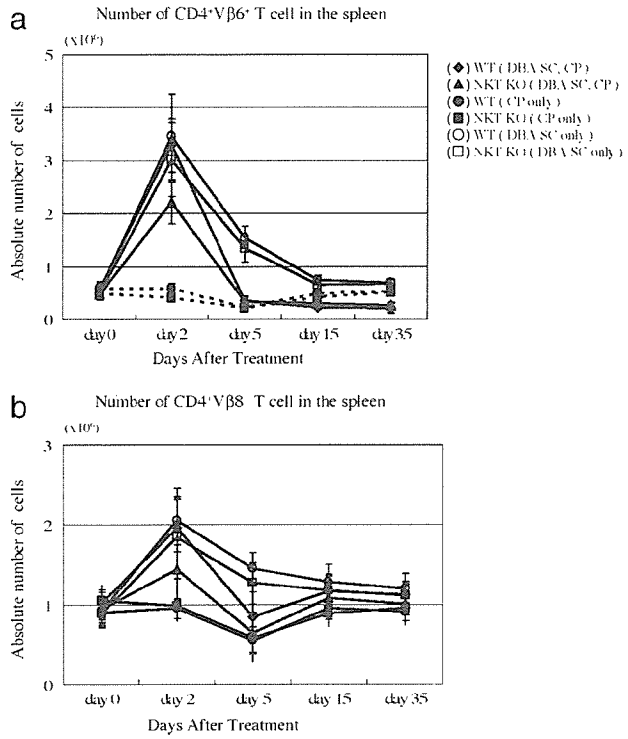

FIGURE 4. Absolute number of cells in the spleen of recipients treated with DBA/2 SC and CP. The kinetics of $CD4^+$ $V\beta6^+$ (*a*) and $CD4^+$ $V\beta8.1/8.2^+$ (*b*) T cells in spleen cells harvested from the recipient BALB/c mice are shown. *a*, The numbers of $CD4^+$ $V\beta6^+$ cells in the spleens from WT mice treated with DBA/2 (DBA) SC and CP (◆; $n = 4$), NKT KO mice treated with DBA/2 SC and CP (▲; $n = 4$), WT mice treated with CP (●; $n = 4$), NKT KO mice treated with CP (■; $n = 4$), WT mice treated with DBA/2 SC (○; $n = 4$), and NKT KO mice treated with DBA/2 SC (□; $n = 4$). *b*, The numbers of $CD4^+V\beta8^+$ cells in the spleens from WT mice treated with DBA/2 SC and CP (◆; $n = 4$), NKT KO mice treated with DBA/2 SC and CP (▲; $n = 4$), WT mice treated with CP (●; $n = 4$), NKT KO mice treated with CP (■; $n = 4$), WT mice treated with DBA/2 SC (○; $n = 4$), and NKT KO mice treated with DBA/2 SC (□; $n = 4$).

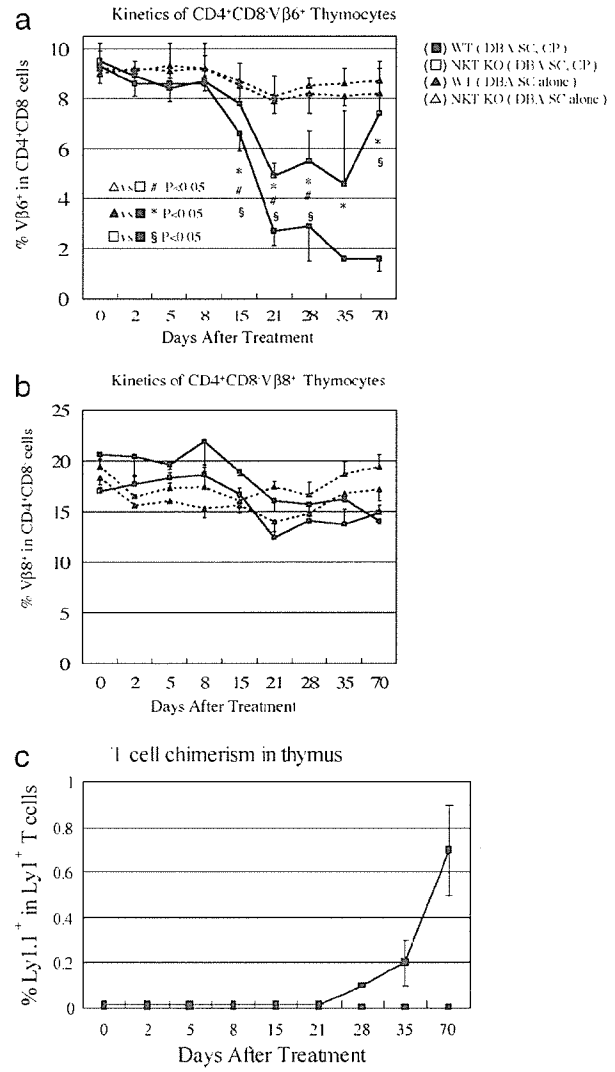

FIGURE 5. Intrathymic clonal deletion in the recipient mice. *a* and *b*, The kinetics of $CD4^+CD8^-V\beta6^+$ (*a*) or $CD4^+CD8^-$ $V\beta8.1/8.2^+$ (*b*) T cells in thymocytes harvested from the recipient BALB/c mice are shown. Thymocytes were labeled with FITC-conjugated anti-Vβ6 or Vβ8.1/8.2 mAb, PE-conjugated anti-CD4 mAb, and allophycocyanin-conjugated anti-CD8 mAb. To determine the percentage of $CD4^+$ T cells that were $V\beta6^+$ or $V\beta8.1/8.2^+$, 10,000–20,000 gated $CD4^+CD8^-$ cells were collected. Thymocytes were obtained from WT mice treated with DBA/2 (DBA) SC and CP (■; $n = 4$), NKT KO mice treated with DBA/2 SC and CP (□; $n = 4$), WT mice treated with DBA/2 SC alone (▲; $n = 4$), and NKT KO mice treated with DBA/2 SC alone (△; $n = 4$). Vertical bars represent SD. The statistical significance of the differences among groups was analyzed and the results are given in *a*. *c*, Intrathymic chimerism in the recipient mice. Thymocytes were labeled with FITC-conjugated anti-Lyt 1.1mAb and PE-conjugated anti-Lyt 1(1.1 + 1.2) mAb. To determine the percentages of T cell chimerism that were Lyt 1.1^+, 10,000–20,000 gated Lyt 1^+ cells were collected. Thymocytes were obtained from WT (Lyt-1.2) mice treated with DBA/2 (Lyt-1.1) SC and CP (■; $n = 4$) and NKT KO mice treated with DBA/2 SC and CP (□; $n = 4$). Chimerism was undetectable in WT or NKT KO mice treated with DBA/2 SC alone (data not shown). Vertical bars represent SD.

decreased to ~3%. The percentage of $CD4^+V\beta6^+$ T cells was significantly reduced in BALB/c WT mice treated with DBA/2 SC and CP as compared with that for BALB/c WT mice treated with DBA/2 SC alone. The disappearance of T cells in WBC was specific for $V\beta6^+$ T cells, because the percentage of $V\beta8.1/8.2^+$ T cells was not significantly altered (Fig. 3*b*). Furthermore, the absolute number of $CD4^+V\beta6^+$ T cells in the spleen was analyzed, and similar results were obtained (Fig. 4). We have already reported this phenomenon, which we termed clonal destruction (12, 13), and similar results were obtained in NKT KO mice treated with DBA/2 SC on day 0 and CP on day 2 (Fig. 4). In contrast, when BALB/c WT or NKT KO mice were treated with CP alone on day 2, a transient reduction of both the $CD4^+V\beta6^+$ and $CD4^+V\beta8^+$ T cell subsets was observed.

To further investigate the cellular events in the thymuses of BALB/c mice made tolerant of DBA/2 mice, the association of the clonal deletion with the mixed chimerism was examined (Fig. 5). Whole thymocytes were stained with FITC-conjugated anti-Vβ6 mAb, PE-conjugated anti-CD4 mAb, and allophycocyanin-conjugated anti-CD8 mAb. We previously reported that intrathymic clonal deletion occurs by 6 wk after SC and CP treatment (12, 13), but we did not investigate whether intrathymic CD4 single-positive T cells are depleted by clonal destruction or when intrathymic clonal deletion begins. The present analysis was performed by gating $CD4^+CD8^-$ single-positive thymocytes.

Among the $CD4^+CD8^-$ thymocytes of the BALB/c WT or NKT KO mice, $CD4^+V\beta6^+$ T cells represented ~9% (Fig. 5*a*),

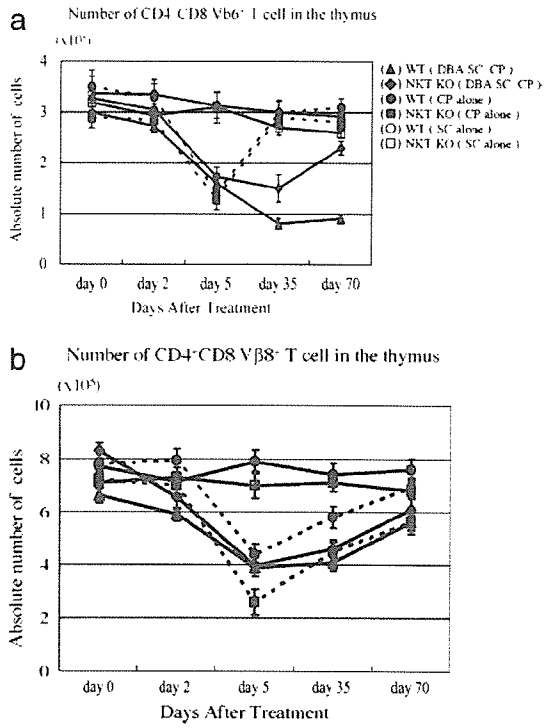

FIGURE 6. Absolute number of cells in the thymuses of recipients treated with DBA/2 (DBA) SC and CP. The kinetics of $CD4^+CD8^-V\beta6^+$ (*a*) and $CD4^+CD8^-$ $V\beta8.1/8.2^+$ (*b*) T cells in thymocytes harvested from the recipient mice are shown. *a*, The numbers of $CD4^+CD8^-V\beta6^+$ cells in the thymuses from WT mice treated with DBA/2 SC and CP (▲; $n = 4$), NKT KO mice treated with DBA/2 SC and CP (◆; $n = 4$), WT mice treated with CP (●; $n = 4$), NKT KO mice treated with and CP (■; $n = 4$), WT mice treated with SC (○; $n = 4$), and NKT KO mice treated with SC (□; $n = 4$). *b*, The numbers of $CD4^+CD8^-V\beta8^+$ cells in the thymuses from WT mice treated with DBA/2 SC and CP (▲; $n = 4$), NKT KO mice treated with DBA/2 SC and CP (◆; $n = 4$), WT mice treated with CP (●; $n = 4$), NKT KO mice treated with CP (■; $n = 4$), WT mice treated with SC (○; $n = 4$), and NKT KO mice treated with SC (□; $n = 4$).

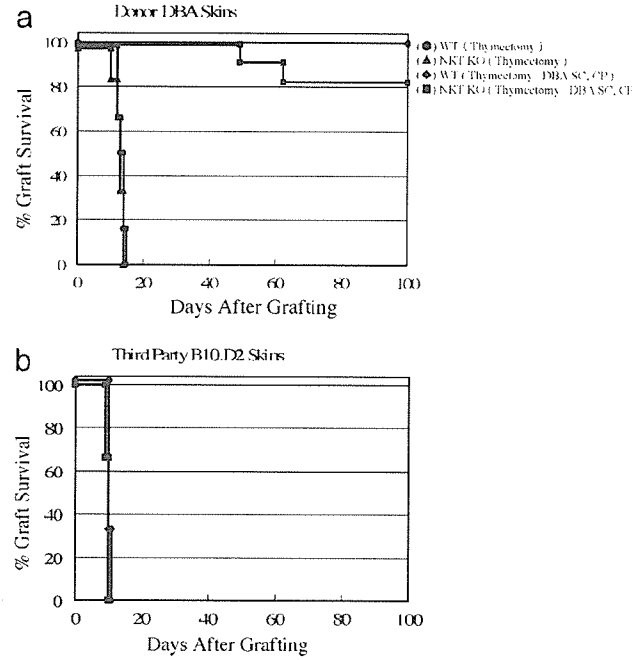

FIGURE 7. Permanent DBA/2 (DBA) skin graft acceptance in the thymectomized BALB/c NKT KO mice treated with DBA/2 SC and CP. Recipient mice were grafted with skin from donor DBA/2 (*a*) or third party B10.D2 (*b*) mice 4 wk after treatment. *a*, The groups and median skin graft survival times were as follows: ●, thymectomized WT mice ($n = 6$; 10 days); ▲, thymectomized NKT KO mice ($n = 6$; 10 days); ◆, thymectomized WT mice treated with DBA/2 SC and CP ($n = 6$; >100 days); ■, thymectomized NKT KO mice treated with DBA/2 SC and CP ($n = 11$; >100 days). *b*, B10.D2 skin grafts were rejected within 14 days after grafting in the following groups: ◆, thymectomized WT mice treated with DBA/2 SC and CP ($n = 3$); and ■, thymectomized NKT KO mice treated with DBA/2 SC and CP ($n = 3$).

and the injection of DBA/2 SC did not significantly alter the percentage of $CD4^+V\beta6^+$ T cells during our observation. In the thymuses of BALB/c WT mice treated with DBA/2 SC and CP, the percentage of $CD4^+V\beta6^+$ T cells was not significantly changed by day 8 but then declined to ~3% by day 21 and reached <2% on day 35. The reduction in $CD4^+V\beta6^+$ T cells was strongly associated with the intrathymic mixed chimerism (Fig. 5c). After 28 days, mixed chimerism was detected in the thymuses of BALB/c WT mice treated with DBA/2 SC and CP. In contrast, in the thymuses of NKT KO mice treated with DBA/2 SC and CP, the percentage of $CD4^+V\beta6^+$ T cells was not significantly changed by day 8, then declined to ~5% on day 21, and returned to the normal range by day 70 (Fig. 5*a*). Mixed chimerism was not detected in the thymuses of BALB/c NKT KO mice treated with DBA/2 SC and CP during our observation (Fig. 5*c*). The intrathymic clonal deletion in the tolerant BALB/c mice was specific for Mls-1^a-reactive T cells expressing TCR Vβ6, because $V\beta8.1/8.2^+$ thymocytes were not deleted (Fig. 5*b*). Furthermore, the absolute number of $CD4^+CD8^-V\beta6^+$ thymocytes was analyzed and similar results were obtained (Fig. 6). When BALB/c WT or NKT KO mice were treated with CP alone on day 2, a transient reduction of both $CD4^+V\beta6^+$ and $CD4^+V\beta8^+$ T cell subsets in the thymus was observed.

Induction of skin allograft prolongation in thymectomized NKT KO mice

The previous results indicated that the effector T cells ($CD4^+CD8^-V\beta6^+$) in the thymuses of WT mice were not depleted until intrathymic clonal deletion occurred and that intrathymic clonal deletion was associated with the establishment of mixed chimerism. Thus, we supposed that the effector T cells generated in the thymus at the early phase of tolerance induction were regulated by NKT cells. To confirm this hypothesis, recipients were thymectomized on day −14. As shown in Fig. 7*a*, DBA/2 skin graft survival was permanently prolonged in 9 of 11 recipient NKT KO mice thymectomized on day −14 and treated with SC on day 0 and CP on day 2 (MST, >100 days). Similar results were obtained in thymectomized WT mice ($n = 6$; MST, >100 days). This skin graft prolongation was tolerogen-specific, because third party B10.D2 ($H\text{-}2^d$) allografts were rejected in a normal fashion (Fig. 7*b*).

Generation of tolerogen-specific regulatory T cells in both WT and NKT KO recipients at the late stage of tolerance

Previous studies have demonstrated that the third mechanism of cyclophosphamide-induced tolerance is a regulatory mechanism at the late stage of tolerance (11, 14). To examine whether NKT cells were involved in the generation of regulatory T cells, adoptive transfer experiments were conducted (Fig. 8). BALB/c WT mice were irradiated with 3 Gy and then received an i.v. transfer of 1×10^8 SC from thymectomized WT or NKT KO recipients that had accepted DBA/2 skin grafts for >100 days. With respect to the T

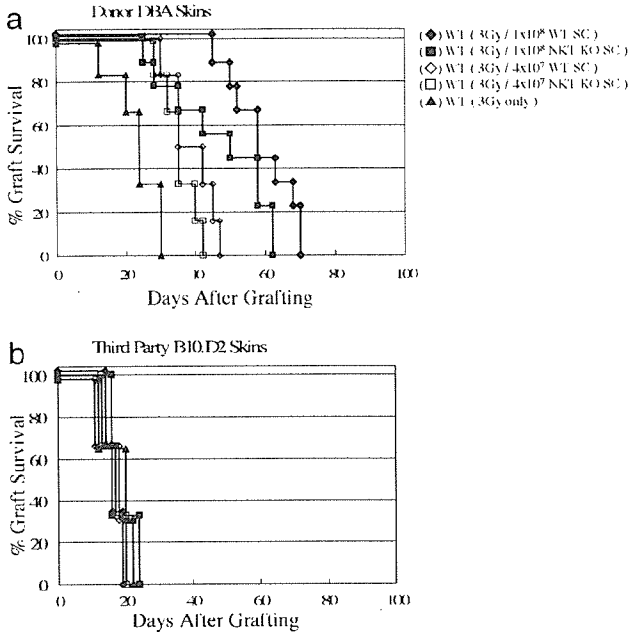

FIGURE 8. Generation of regulatory cells in the recipient mice accepting donor DBA/2 (DBA) skins. BALB/c WT mice were irradiated with 3 Gy and injected i.v. with 1×10^8 or 4×10^7 SC from the thymectomized WT or NKT KO recipients accepting DBA/2 skin grafts >100 days. Recipient mice were grafted with skin from donor DBA/2 (*a*) or third party B10.D2 (*b*) mice 1 day following the transfer of tolerant SC. The groups and median skin graft survival times were as follows: ◆, irradiated WT mice treated with 1×10^8 WT SC (n = 9; 58 days); ■, irradiated WT mice treated with 1×10^8 NKT KO SC (n = 9; 50 days); ◇, irradiated WT mice treated with 4×10^7 WT SC (n = 6; 38.5 days); □, irradiated WT mice treated with 4×10^7 NKT KO SC (n = 6; 35 days); and ▲, irradiated WT mice (n = 6; 24 days). *b*, B10.BR skin grafts were rejected within 24 days after grafting in all groups.

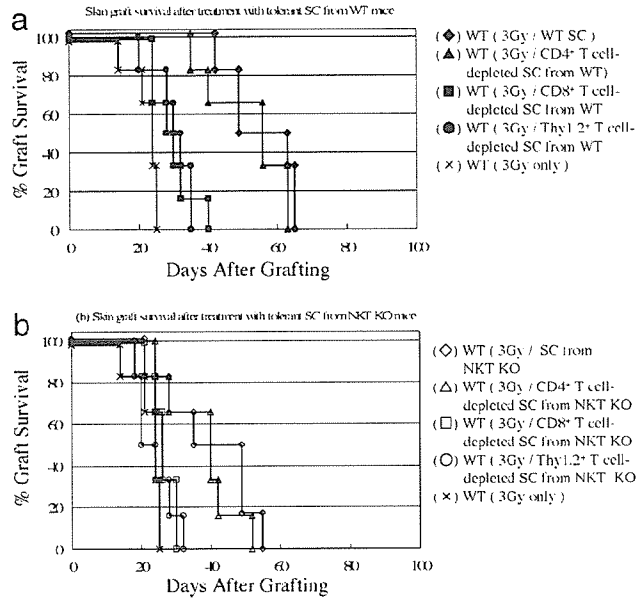

FIGURE 9. Generation of regulatory cells in the recipient mice accepting donor DBA/2 skins. BALB/c WT mice were irradiated with 3 Gy and injected i.v. with 1×10^8 SC from the thymectomized WT or NKT KO recipients accepting DBA/2 skin grafts over 100 days. Recipient mice were grafted with skin from donor DBA/2 mice 1 day following the transfer of tolerant SC. Skin grafting was performed on the same day in all groups. *a*, The groups and median skin graft survival times after treatment with tolerant SC from WT mice were as follows: ◆, irradiated WT mice treated with SC from WT recipients (n = 6; 63 days); ▲, irradiated WT mice treated with $CD4^+$ T cell-depleted SC from WT recipients (n = 6; 56 days); ■, irradiated WT mice treated with $CD8^+$ T cell-depleted SC from WT recipients (n = 6; 29 days); ●, irradiated WT mice treated with $Thy1.2^+$ T cell-depleted SC from WT recipients (n = 6; 32.5 days); and ×, irradiated WT mice (n = 6; 24 days). *b*, The groups and median skin graft survival times after treatment with tolerant SC from NKT KO mice were as follows: ◇, irradiated WT mice treated with SC from NKT KO recipients (n = 6; 42 days); △, irradiated WT mice treated with $CD4^+$ T cell-depleted SC from NKT KO recipients (n = 6; 35 days); □, irradiated WT mice treated with $CD8^+$ T cell-depleted SC from NKT KO recipients (n = 6; 26 days); ○, irradiated WT mice treated with $Thy1.2^+$ T cell-depleted SC from NKT KO recipients (n = 6; 22 days). ×, irradiated WT mice (n = 6; 24 days).

cell percentage of the SC, no significant difference was observed between thymectomized NKT KO mice and BALB/c WT donors (20–25%). Skin grafting was performed 1 day following the transfer of the SC. DBA/2 skin grafts were rejected within 30 days after grafting in the BALB/c WT mice treated with irradiation alone (Fig. 8*a*; n = 6; MST ± SD = 23.3 ± 6.8 days; median = 24 days). The survival of the DBA/2 skin grafts was further prolonged in the irradiated BALB/c WT mice by transferring the SC from thymectomized WT mice that had accepted DBA/2 skin grafts (n = 9; MST ± SD = 59.3 ± 9.1 days; median = 58 days). Similarly, in the irradiated BALB/c WT mice which received the SC transferred from thymectomized NKT KO mice that had accepted DBA/2 skin grafts, the survival of DBA/2 skin grafts was moderately prolonged (n = 9; MST ± SD = 46.7 ± 14.6 days; median = 50 days). There was a statistically significant difference between the graft survivals in irradiated BALB/c WT mice receiving SC transfers from thymectomized WT and NKT KO mice that had accepted DBA/2 skin grafts ($p < 0.05$). In addition, we investigated whether a lower dose of tolerant SC (4×10^7) could induce prolongation of graft survival. Skin graft survival was mildly prolonged in the irradiated BALB/c WT mice by transferring 4×10^7 SC from thymectomized NKT KO mice that had accepted DBA/2 skin grafts (n = 6; MST ± SD = 35.3 ± 5.1 days; median = 35 days). The survival time of the DBA/2 skin grafts was also prolonged in the irradiated BALB/c WT mice by transferring 4×10^7 SC from thymectomized WT mice that had accepted DBA/2 skin grafts (n = 6; MST ± SD = 39.0 ± 6.7 days; median = 38.5 days). In the case of the transfer experiment using low-dose SC, there was no statistically significant difference in survival between the groups treated with 4×10^7 SC from DBA/2 skin graft-accepting thymectomized WT mice and those treated with an equivalent number of SC from DBA/2 skin graft-accepting thymectomized NKT KO mice. The graft survival times in the irradiated BALB/c WT mice treated with a low dose (4×10^7) of SC from DBA/2 skin graft-accepting thymectomized BALB/c WT or NKT KO mice were shorter than those in the irradiated BALB/c WT mice treated with a high dose (1×10^8) of SC. These skin allograft prolongations were tolerogen-specific, because third party skin B10.D2 ($H\text{-}2^d$) allografts were rejected within 24 days after grafting (Fig. 8*b*).

Furthermore, we investigated which T cell subset was dominant in the regulatory function. SC from tolerant BALB/c WT mice were treated with anti-CD4, -CD8, or -Thy-1.2 mAb and complement ex vivo, and 1×10^8 mAb-treated SC were transferred to the irradiated WT mice. Recipient mice were grafted 1 day following the transfer of tolerant SC (Fig. 9*a*). The graft survival time of the recipient treated with $CD4^+$ T cell-depleted SC from tolerant BALB/c WT mice was moderately prolonged (n = 6; MST ±

SD = 52.2 ± 11.9 days; median = 56 days). There was no statistically significant difference compared with the graft survival of the recipient treated with non-T cell-depleted tolerant SC (n = 6; MST ± SD = 55.2 ± 9.7 days; median = 56 days). In contrast, the graft survival of the recipients treated with $CD8^+$ or $Thy1.2^+$ T cell-depleted tolerant SC was significantly shorter than that of the recipients treated with non-T cell-depleted tolerant SC (n = 6; MST ± SD = 29.7 ± 6.0 days; median = 29 days; and n = 6; MST ± SD = 30.0 ± 5.6 days; median = 31 days; respectively). These data indicated that the regulatory cells induced in CP-induced tolerance are mainly $CD8^+$ T cells rather than $CD4^+$ T cells. When SC from tolerant NKT KO mice were used, similar results were obtained (Fig. 9*b*).

Discussion

By using the H-2-matched murine combination of DBA/2 into BALB/c WT and mAbs against T cell markers (Lyt-1.1 and Lyt-1.2) and TCR Vβ6, we have demonstrated the sequential mechanisms of CP-induced tolerance (11, 14). These mechanisms are as follows: 1) clonal destruction of Ag-stimulated and then proliferating T cells by CP at the early stage; 2) intrathymic clonal deletion at the intermediate stage; and 3) regulatory mechanisms at the late stage of tolerance. These three conditions are achieved by SC and 200 mg/kg CP alone without any other supportive treatment in most H-2-matched mouse combinations. In the present study, we have elucidated the roles of NKT cells in the induction of skin allograft tolerance in CP-induced tolerance.

The first mechanism essential to CP-induced tolerance is the selective destruction of Ag-stimulated and then proliferating T cells by CP treatment. This mechanism is considered to be responsible for destroying mature T cells but not immature T cells. As shown in Fig. 3, the $CD4^+V\beta6^+$ T cells that are responsible for the MLR against $Mls\text{-}1^a$-encoded Ag (14) and probably the effector T cells that are responsible for the rejection of DBA/2 skin selectively proliferated on day 2 and were depleted by day 5 in the periphery of the WT mice given DBA/2 SC and CP, leaving most of the nonproliferative $CD4^+V\beta8^+$ T cells. The same results were observed in NKT KO mice given DBA/2 SC and CP, suggesting that NKT-mediated immunoregulation was not required for the induction of clonal destruction in the periphery.

The second mechanism is the intrathymic clonal deletion, which is essential for maintaining the central tolerance in CP-induced tolerance and other chimerism-based tolerance systems (12, 13). By days 28–35 after the treatments with DBA/2 SC and CP, intrathymic chimerism was established due to regeneration of the stem cells of donor origin contained in the tolerogenic SC, and then clonal deletion of $V\beta6^+$ T cells began in the thymuses of WT recipients (Fig. 4). In fact, intrathymic clonal deletion was well correlated with intrathymic mixed chimerism. Notably, in the thymuses of NKT KO recipients given DBA/2 SC and CP, the percentage of $CD4^+V\beta6^+$ T cells decreased only transiently from day 21 through day 35 and returned to the normal level by day 70. Consistently, intrathymic chimerism was not established in NKT KO recipients given DBA/2 SC and CP. Because donor Ag-reactive effector T cells can break mixed chimerism in the periphery, it can be speculated that the effector T cells generated in the thymuses of recipient WT mice by DBA/2 SC administration must be suppressed or regulated by an unsolved mechanism to establish the intrathymic mixed chimerism, which is essential for clonal deletion of donor Ag-specific T cells in the thymus. We hypothesized that this unsolved mechanism could be mediated by the NKT cells. To confirm this hypothesis, we performed a thymectomy and then conditioned the mice with DBA/2 SC and CP (Fig. 7). The results showed that skin graft tolerance was induced in 9 of 11 of the thymectomized NKT KO mice given DBA/2 SC and CP (Fig. 7).

It is important to consider why chimerism or clonal deletion was poorly observed in NKT recipients (group 5; Table I and Fig. 5*a*). Regarding the reduced level of chimerism, we conjectured that chimerism was established by the clonal destruction but was gradually rejected by effector T cells from the thymus. In fact, the level of chimerism was reduced from 2 to 8 wk (group 5; Table I). In BALB/c WT mice, as described above, effector T cells from the thymus were suggested as being regulated by NKT cells, chimerism was stably maintained, and donor skins were permanently accepted. By performing thymectomies in NKT KO mice, a higher level of chimerism could be induced compared with that in non-thymectomized NKT KO mice (group 6 vs 7; Table II). As a result, skin allograft tolerance could be induced in thymectomized NKT KO mice treated with DBA/2 SC and CP. However, the level of chimerism in thymectomized NKT KO mice treated with DBA/2 SC and CP tended to be lower than that in thymectomized BALB/c WT mice treated with DBA/2 SC and CP (group 6 vs group 4; Table II), although this difference did not reach the level of statistical significance. These results may be explained in the following ways. First, we detected T cell chimerism, which may not correlate with bone marrow chimerism. Second, NKT-mediated immunity may contribute to the homeostatic proliferation or self-renewal of T cells. Regarding the poor level of deletion of $CD4^+CD8^-V\beta6^+$ thymocytes in NKT mice (Fig. 5*a*), we can hypothesize that NKT cells may regulate negative selection in the

Table II. *Chimerism and clonal destruction in recipients treated with thymectomy, DBA/2 SC and CP*[a]

Group	Recipient	Treatment[a] Thymectomy (day −14)	SC (day 0)	CP (day 2)	No. of Mice	Chimeric Analysis (percent positive cells ± SD) Lyt-1.1$^+$/Lyt-1$^+$ (%) 2 wk	8 wk	Analysis of TCR Expression (percent positive cells ± SD) $CD4^+V\beta6^+/CD4^+$ (%) 3 wk	9 wk	$CD4^+V\beta6^+/CD4^+$ (%) 3 wk	9 wk
1	BALB/c WT	(+)	(−)	(−)	6	0		11.7 ± 0.9		18.7 ± 2.1	
2	BALB/c NKT KO	(+)	(−)	(−)	6	0		10.1 ± 1.2		18.9 ± 1.5	
3	DBA/2	(+)	(−)	(−)	6	98.0 ± 2.2		0		13.2 ± 2.0	
4	BALB/c WT	(+)	DBA/2	200[b]	6	3.0 ± 1.0[c]	3.5 ± 1.2[c]	1.1 ± 0.2	0.9 ± 0.7	18.7 ± 0.7	16.9 ± 3.3
5	BALB/c WT	Sham	DBA/2	200[b]	6	2.4 ± 0.9	3.2 ± 1.2	1.7 ± 0.4	1.3 ± 0.5	19.2 ± 1.5	17.4 ± 1.1
6	BALB/c NKT KO	(+)	DBA/2	200[b]	6	2.6 ± 0.5[d]	2.0 ± 0.7[d]	1.3 ± 0.3	1.3 ± 0.2	16.2 ± 0.8	14.7 ± 2.4
7	BALB/c NKT KO	Sham	DBA/2	200[b]	6	1.4 ± 0.3	0.8 ± 0.1	1.5 ± 0.5	1.0 ± 0.4	15.9 ± 1.0	16.7 ± 1.3

[a] The recipient mice were primed i.v. with 1×10^8 viable DBA/2 SC on day 0 and then given 200 mg/kg CP on day 2. Thymectomies were performed on some groups on day −14.
[b] Milligrams per kilogram (mg/kg).
[c] No statistical significance as compared with group 6.
[d] $p < 0.01$ compared with group 7.

thymus. We intend to elucidate these unsolved mechanisms in a future study.

The third mechanism is the generation of regulatory cells in the late stage of tolerance (11, 14). Any significant contribution of suppressor factors, such as enhancing Abs or anti-idiotypic Abs, was excluded from the transfer experiments by using the serum from long-term tolerant mice (11). Recent reports have clarified that the regulatory mechanism is mediated by both $CD25^+CD4^+$ and $CD25^-CD4^+$ T cells via CTLA-4 molecules and Th2 cytokines in mAb-induced tolerance systems (23–25). Furthermore, another study has reported that CP depleted $CD25^+CD4^+$ T cells (26). We have reported that $CD8^+$ T cells are generally involved in the suppressor activity in CP-induced tolerance, whereas $CD4^+$ T cells are not (11, 14). The present study confirmed that $CD8^+$ T cells exhibit the main suppressor activity, indicating that $CD25^+CD4^+$ T cells are not involved in the regulatory mechanisms. One of the aims in the present study was to examine the role of NKT cells in the generation of regulatory cells. The results showed that regulatory cells could be generated without the contribution of NKT cells. However, regarding the suppressor activity, NKT may have some effects on the suppression of the alloreactivity in the recipients, because the survival of DBA/2 skin grafts was significantly longer in irradiated recipients receiving a high dose (1×10^8) of SC from tolerant WT mice than in those receiving the same amount of SC from tolerant NKT KO mice.

Two reports have described the critical role of NKT cells in inducing transplantation tolerance (5, 6). However, the precise mechanisms at the cellular and molecular levels have remained unclear. It has been well documented that NKT cells produce large amounts of both IL-4 and IFN-γ upon activation (27–29). Given that IL-4 and IFN-γ have opposite effects on the development of Th1 and Th2 cells, extensive analyses have been performed with various experimental systems, and conflicting results have been reported (30–32). By using IL-4 KO and IFN-γ KO mice, two groups analyzed the mechanisms of the NKT-mediated role in transplantation tolerance induction and produced conflicting results (5, 6). Ikehara et al. (6) suggested that there was little involvement of these two cytokines in C57BL/6 mice injected with anti-CD4 mAb and grafted with rat islets. In contrast, Seino et al. (5) suggested that IFN-γ partially contributes to tolerance induction in C57BL/6 mice injected with anti-LFA-1 and ICAM-1 mAbs and grafted with heart grafts from BALB/c ($H\text{-}2^d$) mice. However, these results did not seem to be definitive, because they could not show clearly whether the IFN-γ produced by NKT cells was involved in one or more of the steps that induce and maintain transplantation tolerance, i.e., activation of effector T cells, apoptosis of effector T cells, reprogramming of effector T cells (anergy induction), and the generation of regulatory T cells. In the present study, we can strongly suggest two roles for NKT cells in CP-induced tolerance. One is to regulate the effector T cells generated in the thymuses of recipient WT mice by DBA/2 SC administration through the establishment of intrathymic clonal deletion. The other is to allow generation of regulatory cells without NKT cell-mediated immunoregulation.

As for the NKT reconstitution assay (Fig. 2), unfortunately we could not show how many NKT cells are needed to completely reconstitute NKT-mediated immunoregulation. In our laboratory, the Vα14 transgenic mice (RAG-1 KO background) needed for reconstituting NKT cells in NKT (Vα14) KO mice are unavailable. However, even in the experiments using the Vα14 transgenic mice, a previous attempt to perform adoptive transfer of $V\alpha14^+$ cells from Vα14 transgenic mice in an allogeneic tolerance system was not successful, probably because the dose of $V\alpha14^+$ cells was not sufficient to restore these cells to the normal level (Y. Yasunami, unpublished observation). We initially transferred 1×10^8 SC from WT mice to NKT KO mice but could not induce permanent acceptance donor skin grafts in three of seven recipients. NKT (αGalCer/CD1d tetramer$^+CD3^+$) cells were restored to 0.4 and 4.3% in SC and LMNC of these mice, respectively, suggesting that the level of NKT reconstitution was not enough. In contrast, Seino et al. had reconstituted WT BMC (including NKT cells and progenitors) in irradiated NKT KO mice (5). To further reconstitute NKT cells, recipient NKT KO mice were irradiated with 3 Gy and reconstituted with SC and BMC from WT mice. Although NKT cells were not fully restored (0.7 and 9.5% in SC and LMNC, respectively), permanent skin graft acceptance was induced in all of the irradiated and reconstituted NKT KO mice.

Acknowledgments

We thank Dr. Hisanori Mayumi, General Manager, Watanabe Hospital (Kagoshima, Japan) for reviewing this manuscript and giving helpful comments. We also thank the Edanz Editing Co. Ltd. (Fukuoka, Japan) and KN International, Inc. (Iowa City, IA) for the English editing of this manuscript.

Disclosures

The authors have no financial conflict of interest.

References

1. Cui, J., T. Shin, T. Kawano, H. Sato, E. Kondo, I. Toura, Y. Kaneko, H. Koseki, M. Kanno, and M. Taniguchi. 1997. Requirement for Vα14 NKT cells in IL-12-mediated rejection of tumors. *Science* 278: 1623–1626.
2. Mieza, M. A., T. Itoh, J. Q. Cui, Y. Makino, T. Kawano, K. Tsuchida, T. Koike, T. Shirai, H. Yagita, A. Matsuzawa, et al. 1996. Selective reduction of $V\alpha14^+$ NK T cells associated with disease development in autoimmune-prone mice. *J. Immunol.* 156: 4035–4040.
3. Slifka, M. K., R. R. Pagarigan, and J. L. Whitton. 2000. NK markers are expressed on a high percentage of virus-specific $CD8^+$ and CD4+ T cells. *J. Immunol.* 164: 2009–2015.
4. Naiki, Y., H. Nishimura, T. Kawano, Y. Tanaka, S. Itohara, M. Taniguchi, and Y. Yoshikai. 1999. Regulatory role of peritoneal $NK1.1^+$ $\alpha\beta$ T cells in IL-12 production during *Salmonella* infection. *J. Immunol.* 163: 2057–2063.
5. Seino, K. I., K. Fukao, K. Muramoto, K. Yanagisawa, Y. Takada, S. Kakuta, Y. Iwakura, L. Van Kaer, K. Takeda, T. Nakayama, et al. 2001. Requirement for natural killer T (NKT) cells in the induction of allograft tolerance. *Proc. Natl. Acad. Sci. USA* 98: 2577–2581.
6. Ikehara, Y., Y. Yasunami, S. Kodama, T. Maki, M. Nakano, T. Nakayama, M. Taniguchi, and S. Ikeda. 2000. $CD4^+$ Vα14 natural killer T cells are essential for acceptance of rat islet xenografts in mice. *J. Clin. Invest.* 105: 1761–1767.
7. Shin, T., H. Mayumi, K. Himeno, H. Sanui, and K. Nomoto. 1984. Drug-induced tolerance to allografts in mice. I. Difference between tumor and skin grafts. *Transplantation* 37: 580–584.
8. Mayumi, H., T. Shin, K. Himeno, and K. Nomoto. 1985. Drug-induced tolerance to allografts in mice II. Tolerance to tumor allografts of large doses associated with rejection of skin allografts and tumor allografts of small doses. *Immunobiology* 169: 147–161.
9. Mayumi, H., K. Himeno, T. Shin, and K. Nomoto. 1985. Drug-induced tolerance to allografts in mice. IV. Mechanisms and kinetics of cyclophosphamide-induced tolerance. *Transplantation* 39: 209–215.
10. Mayumi, H., K. Himeno, K. Tanaka, N. Tokuda, J. L. Fan, and K. Nomoto. 1986. Drug-induced tolerance to allografts in mice. IX. Establishment of complete chimerism by allogeneic spleen cell transplantation from donors made tolerant to H-2-identical recipients. *Transplantation* 42: 417–422.
11. Tomita, Y., H. Mayumi, M. Eto, and K. Nomoto. 1990. Importance of suppressor T cells in cyclophosphamide-induced tolerance to the non-H-2-encoded alloantigens. Is mixed chimerism really required in maintaining a skin allograft tolerance? *J. Immunol.* 144: 463–473.
12. Eto, M., H. Mayumi, Y. Tomita, Y. Yoshikai, and K. Nomoto. 1990. Intrathymic clonal deletion of $V\beta6^+$ T cells in cyclophosphamide-induced tolerance to H-2-compatible, Mls-disparate antigens. *J. Exp. Med.* 171: 97–113.
13. Tomita, Y., Y. Nishimura, N. Harada, M. Eto, K. Ayukawa, Y. Yoshikai, and K. Nomoto. 1990. Evidence for involvement of clonal anergy in MHC class I and class II disparate skin allograft tolerance after the termination of intrathymic clonal deletion. *J. Immunol.* 145: 4026–4036.
14. Eto, M., H. Mayumi, Y. Tomita, Y. Yoshikai, Y. Nishimura, and K. Nomoto. 1990. Sequential mechanisms of cyclophosphamide-induced skin allograft tolerance including the intrathymic clonal deletion followed by late breakdown of the clonal deletion. *J. Immunol.* 145: 1303–1310.
15. Zhang, Q. W., H. Mayumi, M. Umesue, Y. Tomita, K. Nomoto, and H. Yasui. 1997. Fractionated dosing of cyclophosphamide for establishing long-lasting skin allograft survival, stable mixed chimerism, and intrathymic clonal deletion in mice primed with allogeneic spleen cells. *Transplantation.* 63: 1667–1673.
16. Maeda, T., M. Eto, Y. Nishimura, K. Nomoto, and Y. Y. Kong. 1993. Role of peripheral hemopoietic chimerism in achieving donor-specific tolerance in adult mice. *J. Immunol.* 150: 753–762.

17. Yoshikawa, M., Y. Tomita, T. Uchida, Q. W. Zhang, and K. Nomoto. 1999. Lack of pluripotent stem cell engraftment in cyclophosphamide-induced tolerance. *Transplant. Proc.* 31: 898–899.
18. Yoshikawa, M., Y. Tomita, T. Uchida, Q. W. Zhang, I. Shimizu, and K. Nomoto. 1999. Cyclophosphamide 200 mg/kg lacks ability to induce pluripotent stem cell engraftment in mice. *Transplant. Proc.* 31: 1939.
19. Tomita, Y., M. Yoshikawa, Q. W. Zhang, I. Shimizu, S. Okano, T. Iwai, H. Yasui, and K. Nomoto. 2000. Induction of permanent mixed chimerism and skin allograft tolerance across fully MHC-mismatched barriers by the additional myelosuppressive treatments in mice primed with allogeneic spleen cells followed by cyclophosphamide. *J. Immunol.* 165: 34–41.
20. Mayumi, H., K. Nomoto, and R. A. Good. 1988. A surgical technique for experimental free skin grafting in mice. *Jpn. J. Surg.* 18: 548–557.
21. Tomita, Y., A. Khan, and M. Sykes. 1994. Role of intrathymic clonal deletion and peripheral anergy in transplantation tolerance induced by bone marrow transplantation in mice conditioned with a nonmyeloablative regimen. *J. Immunol.* 153: 1087–1098.
22. Matsuda, J. L., O. V. Naidenko, L. Gapin, T. Nakayama, M. Taniguchi, C. R. Wang, Y. Koezuka, and M. Kronenberg. 2000. Tracking the response of natural killer T cells to a glycolipid antigen using CD1d tetramers. *J. Exp. Med.* 192: 741–754.
23. Graca, L., S. Thompson, C. Y. Lin, E. Adams, S. P. Cobbold, and H. Waldmann. 2002. Both $CD4^+CD25^+$ and $CD4^+CD25^-$ regulatory cells mediate dominant transplantation tolerance. *J. Immunol.* 168: 5558–5565.
24. Taylor, P. A., R. J. Noelle, and B. R. Blazar. 2001. $CD4^+CD25^+$ immune regulatory cells are required for induction of tolerance to alloantigen via costimulatory blockade. *J. Exp. Med.* 193: 1311–1318.
25. Kingsley, C. I., M. Karim, A. R. Bushell, and K. J. Wood. 2002. $CD25^+CD4^+$ regulatory T cells prevent graft rejection: CTLA-4- and IL-10-dependent immunoregulation of alloresponses. *J. Immunol.* 168: 1080–1086.
26. Ghiringhelli, F., N. Larmonier, E. Schmitt, A. Parcellier, D. Cathelin, C. Garrido, B. Chauffert, E. Solary, B. Bonnotte, and F. Martin. 2004. $CD4^+CD25^+$ regulatory T cells suppress tumor immunity but are sensitive to cyclophosphamide which allows immunotherapy of established tumors to be curative. *Eur. J. Immunol.* 34: 336–344.
27. Arase, H., N. Arase, K. Ogasawara, R. A. Good, and K. Onoe. 1992. An $NK1.1^+$ $CD4^+8^-$ single-positive thymocyte subpopulation that expresses a highly skewed T-cell antigen receptor Vβ family. *Proc. Natl. Acad. Sci. USA* 89: 6506–6510.
28. Kawano, T., J. Cui, Y. Koezuka, I. Toura, Y. Kaneko, K. Motoki, H. Ueno, R. Nakagawa, H. Sato, E. Kondo, et al. 1997. CD1d-restricted and TCR-mediated activation of Vα14 NKT cells by glycosylceramides. *Science* 278: 1626–1629.
29. Yoshimoto, T., and W. E. Paul. 1994. CD4pos, NK1.1pos T cells promptly produce interleukin 4 in response to in vivo challenge with anti-CD3. *J. Exp. Med.* 179: 1285–1295.
30. Cui, J., N. Watanabe, T. Kawano, M. Yamashita, T. Kamata, C. Shimizu, M. Kimura, E. Shimizu, J. Koike, H. Koseki, et al. 1999. Inhibition of T helper cell type 2 cell differentiation and immunoglobulin E response by ligand-activated Vα14 natural killer T cells. *J. Exp. Med.* 190: 783–792.
31. Burdin, N., L. Brossay, and M. Kronenberg. 1999. Immunization with α-galactosylceramide polarizes CD1-reactive NK T cells towards Th2 cytokine synthesis. *Eur. J. Immunol.* 29: 2014–2025.
32. Singh, N., S. Hong, D. C. Scherer, I. Serizawa, N. Burdin, M. Kronenberg, Y. Koezuka, and L. Van Kaer. 1999. Cutting edge: activation of NK T cells by CD1d and α-galactosylceramide directs conventional T cells to the acquisition of a Th2 phenotype. *J. Immunol.* 163: 2373–2377.

The EMBO Journal (2007) 26, 113–122 | © 2007 European Molecular Biology Organization | All Rights Reserved 0261-4189/07
www.embojournal.org

THE EMBO JOURNAL

Cytoplasmic destruction of p53 by the endoplasmic reticulum-resident ubiquitin ligase 'Synoviolin'

Satoshi Yamasaki[1,14], Naoko Yagishita[1,14], Takeshi Sasaki[1,14], Minako Nakazawa[1,14], Yukihiro Kato[1,14], Tadayuki Yamadera[1,14], Eunkyung Bae[2,14], Sayumi Toriyama[1], Rie Ikeda[1], Lei Zhang[1], Kazuko Fujitani[1], Eunkyung Yoo[2], Kaneyuki Tsuchimochi[1], Tomohiko Ohta[3], Natsumi Araya[1], Hidetoshi Fujita[1], Satoko Aratani[1], Katsumi Eguchi[4], Setsuro Komiya[5], Ikuro Maruyama[6], Nobuyo Higashi[7], Mitsuru Sato[7], Haruki Senoo[7], Takahiro Ochi[8], Shigeyuki Yokoyama[9], Tetsuya Amano[1], Jaeseob Kim[2], Steffen Gay[10], Akiyoshi Fukamizu[11], Kusuki Nishioka[12], Keiji Tanaka[13] and Toshihiro Nakajima[1,*]

[1]Department of Genome Science, Institute of Medical Science, St Marianna University School of Medicine, Kawasaki, Japan, [2]GenExl, Inc. Biomedical Research Center, Taejon, South Korea, [3]Division of Breast and Endocrine Surgery, Institute of Medical Science, St Marianna University School of Medicine, Kawasaki, Japan, [4]The First Department of Internal Medicine, Nagasaki University School of Medicine, Nagasaki, Japan, [5]Department of Orthopedic Surgery, Kagoshima University, Faculty of Medicine, Kagoshima, Japan, [6]Department of Dermatology and Laboratory of Molecular Medicine, Kagoshima University, Faculty of Medicine, Kagoshima, Japan, [7]Department of Anatomy, Akita University School of Medicine, Akita, Japan, [8]National Hospital Organization Sagamihara National Hospital, Kanagawa, Japan, [9]Department of Biophysics and Biochemistry, Graduate School of Science, University of Tokyo, Tokyo, Japan; Protein Research Group, RIKEN Genomic Sciences Center, Yokohama, Japan, [10]Department of Rheumatology, University Hospital Zürich, Zürich, Switzerland, [11]Aspect of Functional Genomic Biology, Center of Tsukuba Advanced Research Alliance, University of Tsukuba, Tsukuba, Japan, [12]Rheumatology, Immunology and Genetics Program, Institute of Medical Science, St Marianna University School of Medicine, Kawasaki, Japan and [13]Laboratory of Frontier Science, The Tokyo Metropolitan Institute of Medical Science, Tokyo, Japan

Synoviolin, also called HRD1, is an E3 ubiquitin ligase and is implicated in endoplasmic reticulum -associated degradation. In mammals, Synoviolin plays crucial roles in various physiological and pathological processes, including embryogenesis and the pathogenesis of arthropathy. However, little is known about the molecular mechanisms of Synoviolin in these actions. To clarify these issues, we analyzed the profile of protein expression in *synoviolin*-null cells. Here, we report that Synoviolin targets tumor suppressor gene p53 for ubiquitination. Synoviolin sequestrated and metabolized p53 in the cytoplasm and negatively regulated its cellular level and biological functions, including transcription, cell cycle regulation and apoptosis. Furthermore, these p53 regulatory functions of Synoviolin were irrelevant to other E3 ubiquitin ligases for p53, such as MDM2, Pirh2 and Cop1, which form autoregulatory feedback loops. Our results provide novel insights into p53 signaling mediated by Synoviolin.

The EMBO Journal (2007) **26**, 113–122. doi:10.1038/sj.emboj.7601490; Published online 14 December 2006
Subject Categories: proteins
Keywords: apoptosis; cell growth; E3 ubiquitin ligase; endoplasmic reticulum-associated degradation; rheumatoid arthritis

Introduction

The ubiquitin–proteasome system (UPS) consists of a small polypeptide ubiquitin, a framework of enzymes that mediates the covalent attachment of ubiquitin to proteolytic substrates and the 26S proteasome that digests the modified proteins into peptides. The formation of ubiquitin conjugates requires the successive action of three classes of enzymes. This process is first activated by an E1 (activating enzyme) in an ATP-dependent manner, forming a high-energy thioester bond between ubiquitin and an E1, and the activated ubiquitin is then transferred to an E2 (conjugating enzyme), forming a similar thioester linkage between ubiquitin and E2, and then E3 ubiquitin ligase transfers ubiquitin to the target proteins. Through repeated reactions of this cycle, a polyubiquitin chain is formed on the target proteins, which is recognized by the 26S proteasome for ultimate degradation (Hershko and Ciechanover, 1998; Pickart, 2001). In the UPS pathway, the E3 ubiquitin ligases play critical roles in the selection of target proteins for degradation, because each distinct E3 ubiquitin ligase usually binds a protein substrate with a degree of selectivity for ubiquitination in a temporally and spatially regulated fashion.

Synoviolin, a representative of endoplasmic reticulum (ER)-resident E3 ubiquitin ligases, is a mammalian homolog of Hrd1p/Der3p that "substrates" misfolded carboxypeptide yscY (CPY*) (Bordallo *et al*, 1998) and 3-hydroxy-3-methylglutaryl-coenzyme A reductase (HMGR), a key enzyme of the mevalonate pathway in yeast (Shearer and Hampton, 2004, 2005). We cloned Synoviolin from rheumatoid synovial cells (RSCs) and described that Synoviolin is highly expressed in synoviocytes of patients with rheumatoid arthritis (RA) (Amano *et al*, 2003). In that report, we demonstrated that overexpression of Synoviolin in transgenic mice leads to advanced arthropathy caused by reduced apoptosis of synoviocytes. On the other hand, *synoviolin*$^{+/-}$ mice showed resistance to the development of arthritis owing to enhanced

*Corresponding author. Department of Genome Science, Institute of Medical Science, St Marianna University School of Medicine, 2-16-1 Sugao Miyamae-ku, Kawasaki, Kanagawa 216-8512, Japan. Tel.: +81 44 977 8111 (ext. 4111); Fax: +81 44 977 10712; E-mail: nakashit@marianna-u.ac.jp
[14]These authors contributed equally to this work

Received: 11 April 2006; accepted: 7 November 2006; published online: 14 December 2006

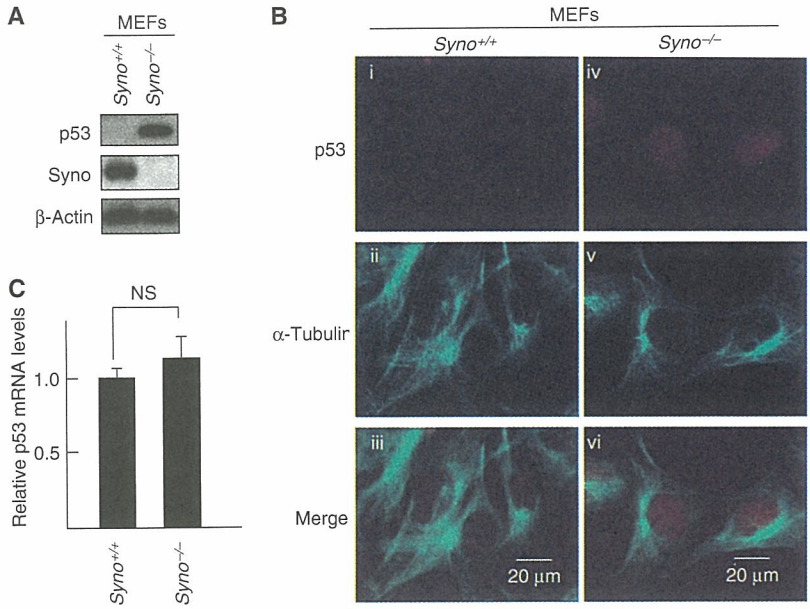

Figure 1 Accumulation of p53 in *synoviolin* null cells. (**A**) Accumulation of p53 in $Syno^{-/-}$ MEFs. (**B**) Nuclear accumulation of p53 in $Syno^{-/-}$ MEFs. p53 in $Syno^{+/+}$ MEFs (i–iii) and $Syno^{-/-}$ MEFs (iv–vi). Merged images are shown in the bottom panels (iii, vi). (**C**) Quantification of p53 mRNA. The *p53* mRNA level was assessed by real-time PCR and normalized to 18S rRNA. Data are mean±s.e.m. of four experiments. Statistical analysis using Student *t*-test indicated no significant difference between $Syno^{+/+}$ and $Syno^{-/-}$ MEFs (NS).

apoptosis of synovial cells. These results indicate that Synoviolin is a novel causative factor for arthropathy based on its anti-apoptotic effects. In another study, we reported that all mice fetuses lacking *synoviolin* ($Syno^{-/-}$) died *in utero* around E13.5 (Yagishita *et al*, 2005), although Hrd1p/Del3p, a yeast ortholog of Synoviolin, was described as non-essential for survival. $Syno^{-/-}$ were anemic owing to enhanced apoptosis of fetal liver cells (Yagishita *et al*, 2005). It is surprising that an ER-associated degradation (ERAD)-associated E3 ubiquitin ligase, Synoviolin, is involved in cell hyperplasia of dividing cells via its anti-apoptotic effect. In this regard, like RSCs, the anti-apoptotic effect of Synoviolin was observed even for *synoviolin* expressed ectopically in NIH3T3 cells, which resulted in enhanced cell overgrowth in these cells (Tsuchimochi *et al*, 2005). These results were confirmed also in the *Drosophila* fly (Supplementary Figure 1). An important question remains unanswered at this stage. What is the mechanism of Synoviolin-induced cell overgrowth? The present study was designed to identify the substrates for Synoviolin that may be involved in cell growth.

Results

Accumulation of p53 in synoviolin-null cells

To identify target(s) for Synoviolin, we assumed that the lack of Synoviolin results in accumulation of substrate proteins. First, we carried out a two-dimensional polyacrylamide gel electrophoresis (PAGE) using mouse embryonic fibroblasts (MEFs) of $Syno^{-/-}$. In these experiments, p53 was identified as one of the major targets in the profile by LC-MAS analysis (Supplementary Figure 2). Indeed, the level of p53 was markedly enhanced in $Syno^{-/-}$ MEFs (Figure 1A) and $Syno^{-/-}$ embryos, especially in the posterior part of the body such as somites, brains and maxillary or branchial arches (Supplementary Figure 3), as reported previously (Gottlieb *et al*, 1997). The accumulated p53 was predominantly localized in the nuclei of $Syno^{-/-}$ MEFs (Figure 1B), although the mRNA level of *p53* was not altered in $Syno^{-/-}$ MEFs (Figure 1C). Phosphorylation of p53 was not observed in $Syno^{-/-}$ MEFs (Supplementary Figure 4).

Increment of functional p53 in synoviolin-null cells

Next, we tested whether impairment of Synoviolin influences the functions of p53 in the cell. Knockdown of Synoviolin by small interfering RNA (siRNA) for *synoviolin* (*Syno* siRNA) in RKO cells, a human colon cancer cell line known to express wild-type (WT) p53 (Smith *et al*, 1995), resulted in almost complete disappearance of Synoviolin expression (Figure 2A). Synoviolin knockdown was associated with increased p53 protein level and nuclear accumulation of p53 (Figure 2A and B), but no change in p53 mRNA levels (Figure 2C). No changes were noted in the expression levels of other ubiquitin ligases for p53 such as MDM2, Arf-BP (data not shown) and Parc (see Figure 4B), in *synoviolin*-null RKO cells (Brooks and Gu, 2006). On the other hand, the expression levels of unfolded protein response (UPR) markers such as HERP and PERK (Wu and Kaufman, 2006) were increased, which suggests that accumulation of unfolded proteins in *synoviolin*-knockdown RKO cells caused ER stress, followed by UPR (data not shown). These results were confirmed in other cell lines (HEK293 cells and HeLa cells, data not shown). In another experiment, a marked increase was noted in the binding of p53 to its consensus sequences such as *GADD45*, *MDM2* and *p21* promoter in *synoviolin*-knockdown cells compared with *GFP*-knockdown cells (Figure 2D). Furthermore, further additions of the respective competitor abrogated the binding capacity dose-dependently, confirming the specific interactions of p53 on electrophoretic mobility

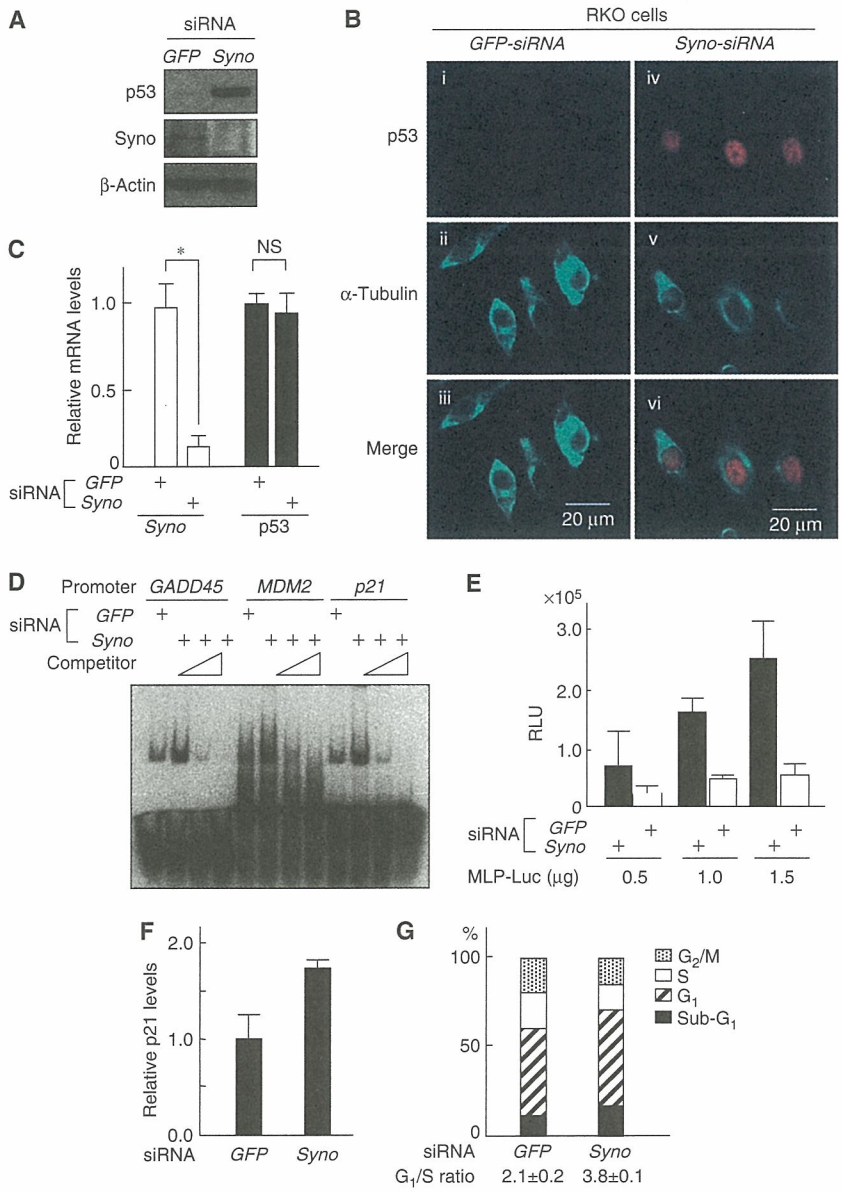

Figure 2 Functional evaluation of increased p53 in *synoviolin*-deficient RKO cells. (**A**) Increment of endogenous p53 by depletion of *synoviolin*. (**B**) Depletion of *synoviolin* causes nuclear accumulation of p53. Merged images are shown in the bottom panels (iii, vi). (**C**) *synoviolin* depletion does not affect mRNA levels of *p53*. Real-time PCR was performed as in Figure 1C. $^*P<0.01$. (**D**) DNA-binding activity of p53 for promoters of the indicated genes increases by depletion of *synoviolin*. (**E**) Transactivation activity of p53 is increased upon depletion of Synoviolin. Relative transactivation activity was determined by normalizing luciferase to an internal control, β-Gal activity from RSV-β-gal plasmid. RLU, relative light units. (**F**) siRNA depletion of *synoviolin* causes activation of p21 expression. (**G**) siRNA-induced depletion of *synoviolin* induces G_1 arrest. The cell-cycle profile was determined by propidium iodide staining and FACS. The results represent the average of triplicate experiments. Data in (C), (E) and (F) are mean±s.e.m. of four experiments.

shift assay (EMSA) (Figure 2D). We also noted three times increment of luciferase activities on *GADD45*-MLP-Luciferase reporter plasmid in *synoviolin*-deficient RKO cells compared with *GFP*-siRNA-treated RKO cells (Figure 2E). Moreover, in *Syno* siRNA-treated RKO cells, we detected enhanced expression of p21, one of the target genes of p53 (Figure 2F), and the accumulation of cells in G_1 phase and decreased cells in S phase (Figure 2G). Taken together, the above results indicate that Synoviolin deficiency is not only associated with increased levels of p53, but also with functional activation of p53.

Synoviolin sequestrates p53 in the cytoplasm

To understand the molecular mechanism of Synoviolin-induced control of p53, we investigated the interaction between Synoviolin and p53 *in vitro*. As shown in Figure 3A, GST-SynoΔTM interacted directly with p53 (lane 8). A series of N-terminus Synoviolin-TM deletion mutants showed that the amino-acid sequence 236–270 of Synoviolin is responsible for binding with p53 (lanes 1–6) (this binding domain was termed provisionally as '53BD'). Furthermore, a synthetic 53BD peptide inhibited Synoviolin-p53 interaction in a dose-

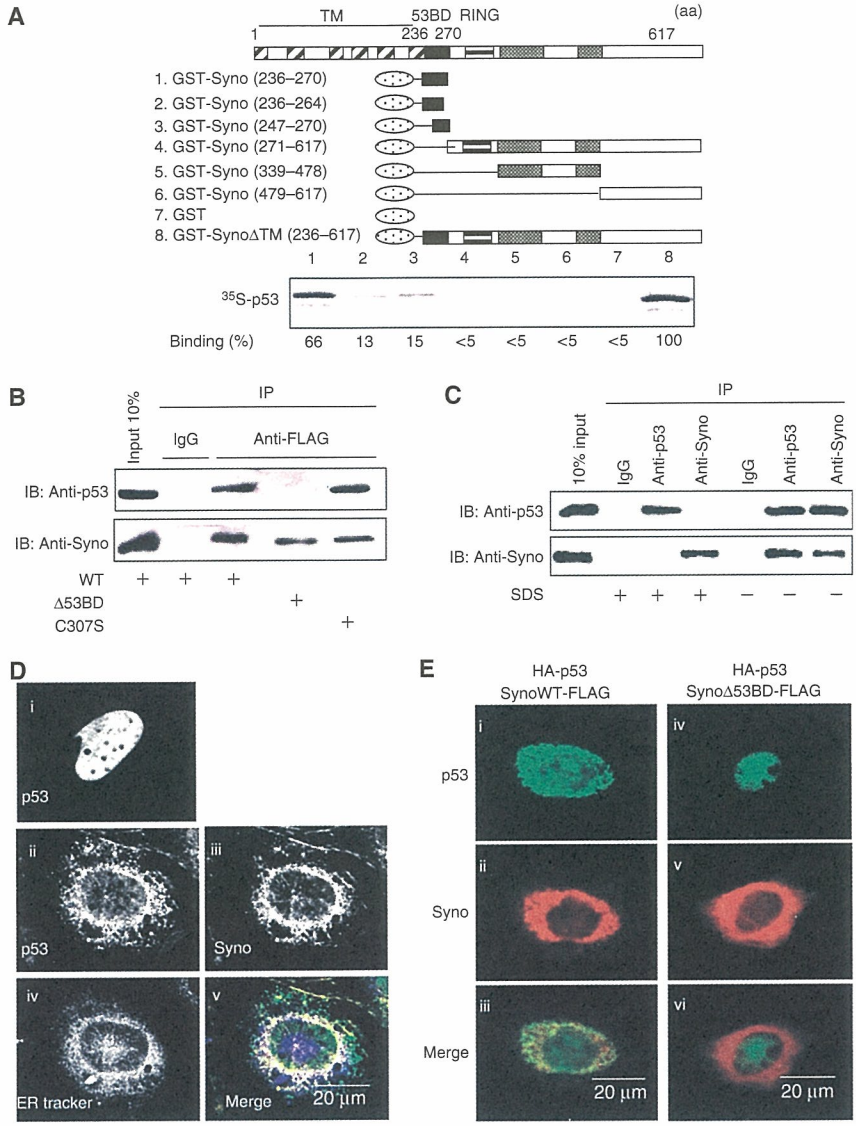

Figure 3 Synoviolin sequestrates p53 in the ER through its 53BD-dependent interaction with p53. (**A**) Identification of p53-binding domain of Synoviolin *in vitro*. Black box: p53-binding domain (53BD), gray box: proline-rich domain, oval box: GST. Relative binding ability is denoted as percentage (100% = SynoΔTM, lane 8). (**B**) 53BD-dependent *in vivo* binding of Synoviolin with p53 in HEK293 cell. (**C**) Interaction between endogenous Synoviolin and p53 in HEK293 cells. Cell lysates were immunoprecipitated in the presence or absence of SDS by using anti-p53 antibodies, anti-Synoviolin antibodies or control IgG. Inputs and immunoprecipitates were analyzed by Western blot by using anti-p53 or anti-Synoviolin antibodies. (**D**) P53 is anchored around ER in a Synoviolin-dependent manner. Saos-2 cells were transfected with HA-p53 (i) or co-transfected with HA-p53 and Synoviolin-FLAG (ii–v). Panel v shows a merged image with p53 (green), Synoviolin (red) and ER-Tracker stain (blue). (**E**) Binding of p53 with Synoviolin is required for p53 anchoring in the ER. Saos-2 cells were co-transfected with HA-p53 and Synoviolin WT-FLAG (I–iii) or SynoviolinΔ53BD-FLAG (iv–vi). Merged images are shown in the bottom panels (iii, vi).

dependent manner, whereas a peptide representing amino acids 322–332 of Synoviolin, used as a negative control, did not show any inhibitory activity (Supplementary Figure 5). We also confirmed *in vivo*, using co-immunoprecipitation assay, the interaction of transiently expressed exogenous Synoviolin WT-FLAG and p53, and the necessity of 53BD was also apparent (Figure 3B). The interaction of these two molecules was independent of ubiquitin ligase activity of Synoviolin, because Synoviolin C307S-FLAG lacking E3 activity bound to p53, as its WT (Figure 3B). Furthermore, endogenous interaction of p53 and Synoviolin was also confirmed in HEK293 cells (Figure 3C).

Considering the interplay between the ER-resident Synoviolin and the nuclear p53, we next investigated their cellular localization in Saos-2 cells, a human osteosarcoma cell line that lacks the endogenous p53 gene (Fogh *et al*, 1977), under conditions of transient expression of exogenous HA-p53 with Synoviolin WT-FLAG or SynoviolinΔ53BD-FLAG (Figure 3D and E). By overexpression of HA-p53 alone in these cells, HA-p53 was localized in the nucleus (Figure 3Di), as reported previously (Shaulsky *et al*, 1990). On the other hand, when HA-p53 was coexpressed with Synoviolin WT-FLAG, HA-p53 was predominantly colocalized with Synoviolin WT-FLAG in the perinuclear regions, but not in

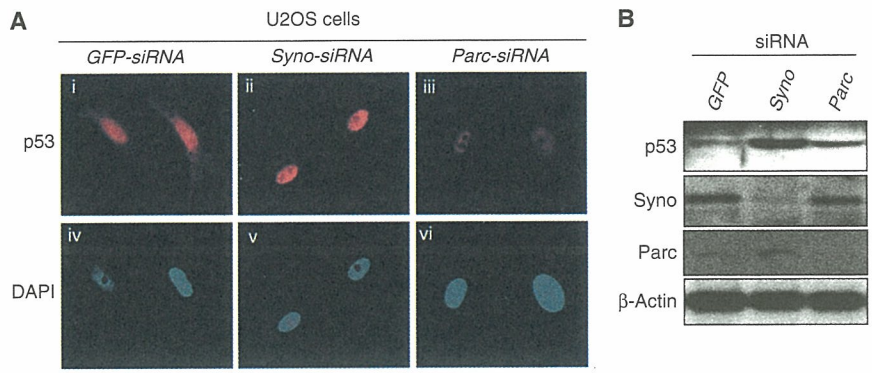

Figure 4 p53-related functional differences between Synoviolin and Parc. (**A**) Nuclear accumulation of p53 by knockdown of *synoviolin* or *Parc*. (**B**) Different levels of p53 following knockdown of *synoviolin* compared with *Parc*.

the nucleus (Figure 3Dii, iii and v). The perinuclear regions were confirmed to be the ER, by counterstaining with ER-Tracker Blue-White DPX (Figure 3Div and v). In addition, ectopically expressed SynoviolinΔ53BD-FLAG did not affect the translocation of HA-p53 into the nucleus (Figure 3E). These results clearly indicate that Synoviolin entraps p53 around ER, and that 53BD is required for this sequestration *in vivo*. In this regard, a previous study reported that another RING finger protein, Parc (Nikolaev *et al*, 2003), also acts as a cytoplasmic anchor for p53. To compare the characteristics of Synoviolin and Parc, we investigated p53 localization in U2OS cells, a human osteosarcoma cell line known to express WT p53 (Ponten and Saksela, 1967), after depletion of *synoviolin* or *Parc* (Nikolaev *et al*, 2003). Treatment with either *Syno* siRNA (Figure 4Aii and v) or *Parc* siRNA (Figure 4Aiii and vi) resulted in accumulation of p53 in the nucleus with diffused and lesser staining in the cytoplasm, different from treatment with *GFP* siRNA. Whereas the nuclear translocation of p53 was comparable in both *Syno* siRNA and *Parc* siRNA cells, a higher expression of p53 was observed in *synoviolin*-deficient U2OS cells (Figure 4Aii and iii). Western blotting analysis also revealed increased level of p53 in Synoviolin-knockdown but not in Parc-knockdown cells (Figure 4B). These findings indicate that Synoviolin regulates both localization and quantity of p53, whereas Parc does not affect the amount of p53, as reported previously (Nikolaev *et al*, 2003).

Synoviolin functions as a novel E3 ubiquitin ligase for p53 degradation

Considering that Synoviolin interacts with p53 *in vitro* and *in vivo*, we next examined whether Synoviolin ubiquitinates p53. As shown in Figure 5A, polyubiquitinated GST-p53 was detected only in the presence of ATP, PK-His-HA-Ub, E1, E2 (UbcH5c) and SynoviolinΔTM (SynoΔTM). This activity was not observed when we used Synoviolin with mutation in the RING finger domain (Figure 5B), and the deletion of 53BD also did not show any ubiquitination activity on p53 (Figure 5B), but this mutant by itself still preserved the auto-ubiquitination activity (Supplementary Figure 6). In addition, the 53BD peptide also inhibited polyubiquitination of p53 compared with a control peptide (amino acids 322–332), although the 53BD peptide did not influence the auto-ubiquitination activity of Synoviolin (Supplementary Figure 7). Moreover, ubiquitinated FLAG-p53 was observed when HA-tagged ubiquitin and Synoviolin WT were coexpressed in HEK293 cells because of its easy transfection, but Synoviolin C307S did not (Figure 5C). As a positive control, p53 was ubiquitinated by MDM2 in an *in vivo* ubiquitination assay (Figure 5C) (Haupt *et al*, 1997; Kubbutat *et al*, 1997).

In the next step, we tested the implication of ubiquitination of p53 by Synoviolin in the degradation of p53 *in vivo*. In HEK293 cells, overexpressed Synoviolin WT significantly shortened the half-life of endogenous p53, whereas Synoviolin C307S and SynoviolinΔ53BD did not increase the degradation rate of p53 (Figure 5D top, mock: 125.5±18.2 min, Synoviolin WT: 44.8±3.8 min, Synoviolin C307S: 177.3±26.8 min and SynoviolinΔ53BD: 161.0±41.4 min). These results indicate that Synoviolin is responsible for the turnover of p53 as its E3 ubiquitin ligase *in vivo*. Consistent with these data, the half-life of p53 was significantly prolonged in $Syno^{-/-}$ MEFs (Figure 5D (bottom), $Syno^{+/+}$ MEFs: 26.1±1.6 min; and $Syno^{-/-}$ MEFs: 120.0±30.3 min. $P<0.05$) as well as RKO cells treated with *synoviolin* siRNA (Supplementary Figure 8). In this regard, several ubiquitin ligases, such as *Cop1* (Dornan *et al*, 2004), *Pirh2* (Leng *et al*, 2003) and *MDM2* (Haupt *et al*, 1997; Kubbutat *et al*, 1997), are already reported to negatively regulate p53 (Bode and Dong, 2004). To ascertain the significance of Synoviolin relative to these ligases, we compared the effects of depletion of *synoviolin* and/or *Cop1*, *Pirh2* or *MDM2* on the expression level of p53 in RKO cells. The amount of p53 by *synoviolin* ablation was less than that by *MDM2* ablation, but equivalent to that by *Cop1* ablation. Depletion of *synoviolin* in cells treated with siRNA for *Cop1*, *Pirh2* or *MDM2* non-redundantly increased p53 levels (Figure 5E). Therefore, Synoviolin functionally targets p53 independent of other ubiquitin ligase pathways. Then, does Synoviolin regulate p53 activation process? To address this question, we applied genotoxic stress as a stimulus for p53 activation (Kastan *et al*, 1991; Vogelstein *et al*, 2000). *Syno* siRNA and *GFP* siRNA-transfected RKO cells were treated with or without genotoxic stresses such as camptothecin, actinomycin D and γ-irradiation. As expected, increased level of p53 by Synoviolin knockdown was cooperatively enhanced by treatment with genotoxic stresses in these cells (Figure 5F). Thapsigargin induced Synoviolin expression, as reported previously (Yagishita *et al*, 2005),

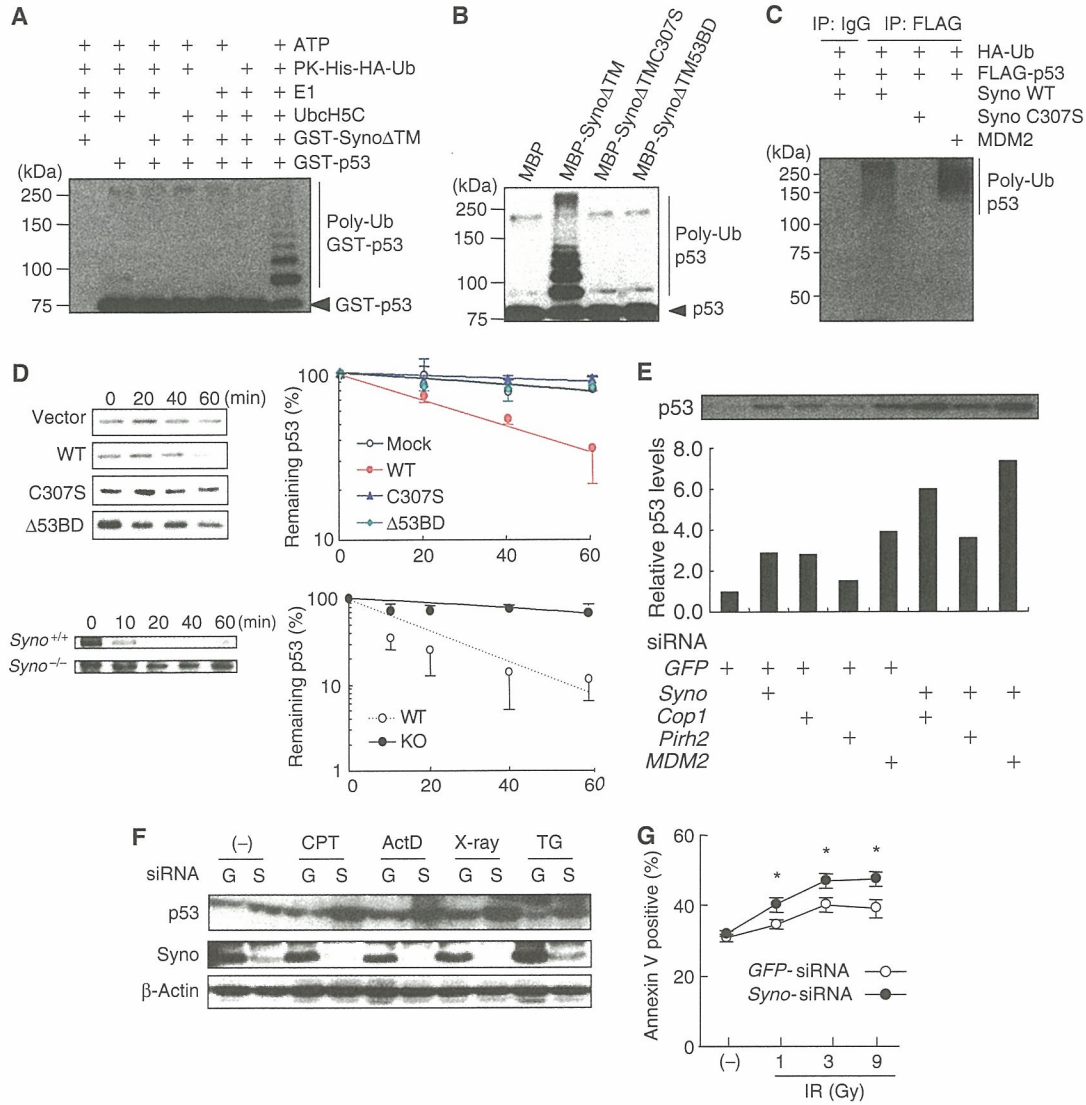

Figure 5 Synoviolin up-regulates p53 level in cells under normal and genotoxic stress conditions. (**A**) Synoviolin ubiquitinates p53 *in vitro*. (**B**) The ubiquitination of p53 is dependent on an intact RING finger domain. (**C**) WT Synoviolin, but not RING finger mutant, ubiquitinates p53 *in vivo*. (**D**) Synoviolin over-expression in HEK293 cells increases degradation of p53 (top). At 24 h after the transfection with empty vector, wild type Synoviolin (WT), mutants in RING finger domain (C307S) or p53 binding domain deletion mutant (Δ53BD), p53 expression was examined at indicated time of cycloheximide treatment. Degradation of p53 is inhibited in synoviolin knockout MEFs ($Syno^{-/-}$) compared with wild type MEFs ($Syno^{+/+}$). The p53 expression was examined after the indicated time of cycloheximide treatment. The remaining p53 expressions were normalized to β-actin expression and plotted against time (minutes). (**E**) Effects of knockdown of Synoviolin and/or other known E3 ubiquitin ligases for p53 on the level of p53 in RKO cells. Quantified p53 level is expressed as relative levels (1.0 = *GFP*-siRNA treated RKO cells). (**F**) Genotoxic stress induces p53 accumulation in the absence of Synoviolin. *GFP*- siRNA (G). *syno* siRNA (S). At 48 h after transfection, the RKO cells were treated with vehicle, camptothecine (CPT, 0.5 μM), actinomycin D (ActD, 5 nM), X-Ray (9 Gray) or thapsigargin (TG, 1 μM) for 6 h. (**G**) Synoviolin knockdown sensitizes cells to genotoxic stress. At 48 h after transfection, cells were exposed to the indicated doses of ionizing-radiation for 24 h, followed by FACS analysis to detect annexin V-positive cells. Data in (D) and (G) are mean ± s.e.m. of $n \geqslant 3$. $^*P < 0.05$.

which was abolished in *Syno* siRNA-transfected RKO cells (Figure 5F). Consistent with the findings of a previous report (Qu *et al*, 2004), thapsigargin, an ER stress inducer, destabilized p53 expression compared with vehicle treatment in *GFP* siRNA-treated RKO cells. Interestingly, the thapsigargin-induced inhibition of p53 expression was reversed, at least in part, by the ablation of Synoviolin (Figure 5F). In addition, the sensitivity of *syno* siRNA-treated RKO cells to γ-irradiation was significantly increased compared with *GFP* siRNA-treated RKO cells (Figure 5G). Considered together, these results indicate that Synoviolin also participates in genotoxic stress response through the mechanism identified here.

Synoviolin regulates p53-dependent apoptotic pathway in vivo

The above experiments provided several pieces of evidence that Synoviolin is a novel class of E3 ubiquitin ligase for p53. However, the majority of the results obtained from cultured cells may not fully reflect the physiological function of p53 in

the context of the whole organism. Therefore, we used *Drosophila* to confirm the association between Synoviolin and p53. Among *Drosophila* clones, CG1937 was identified by BLASTP (protein–protein blast analysis using flybase—http://flybase.bio.indiana.edu/blast/) as the gene with 63% homology to mammalian Synoviolin, and the RING domain of CG1937 is highly conserved (82%) and *in vitro* ubiquitination assay evidently indicated that *Drosophila* Synoviolin (dSyno) ubiquitinates *Drosophila* p53 (Dmp53) (Figure 6A) (Ollmann *et al*, 2000). To investigate the role of Synoviolin in p53 regulation in the whole organism, we generated transgenic flies in which Dmp53 or dSyno was overexpressed by tissue-specific Gal4 driver (Harrison *et al*, 1995). By crossing each transgenic fly, we generated e16E-Gal4/UAS-Dmp53;UAS-dSyno/+ flies, in which both Dmp53 and dSyno could be overexpressed in the posterior halves of wings by e16E-Gal4 driver. The expression level of Dmp53 in the wing discs was significantly decreased in e16E-Gal4/UAS-Dmp53;UAS-dSyno/+ discs compared with e16E-Gal4/Dmp53;+/+ discs (Figure 6B). Moreover, acridine orange staining of apoptotic cells in these discs demonstrated that the level of apoptosis induced by overexpression of Dmp53 was diminished by dSyno overexpression (Figure 6C). These results indicate that dSyno affects Dmp53 protein levels in the fly system, similar to the results of the cell culture system.

In addition to decreased Dmp53 protein level by dSyno in the wing discs of adult flies, dSyno altered the wing phenotype. Namely, overexpression of Dmp53 by e16E-Gal4 driver caused bubbled wing phenotype at the posterior half of wings (Figure 6Di). This phenotype was completely suppressed by dSyno overexpression (Figure 6Dii and Supplementary Table 1). Overexpression of dSyno alone by e16E-Gal4 driver also produced wing phenotype (weak wrinkling of the posterior edge of the wing) (Figure 6Diii). This wrinkled phenotype

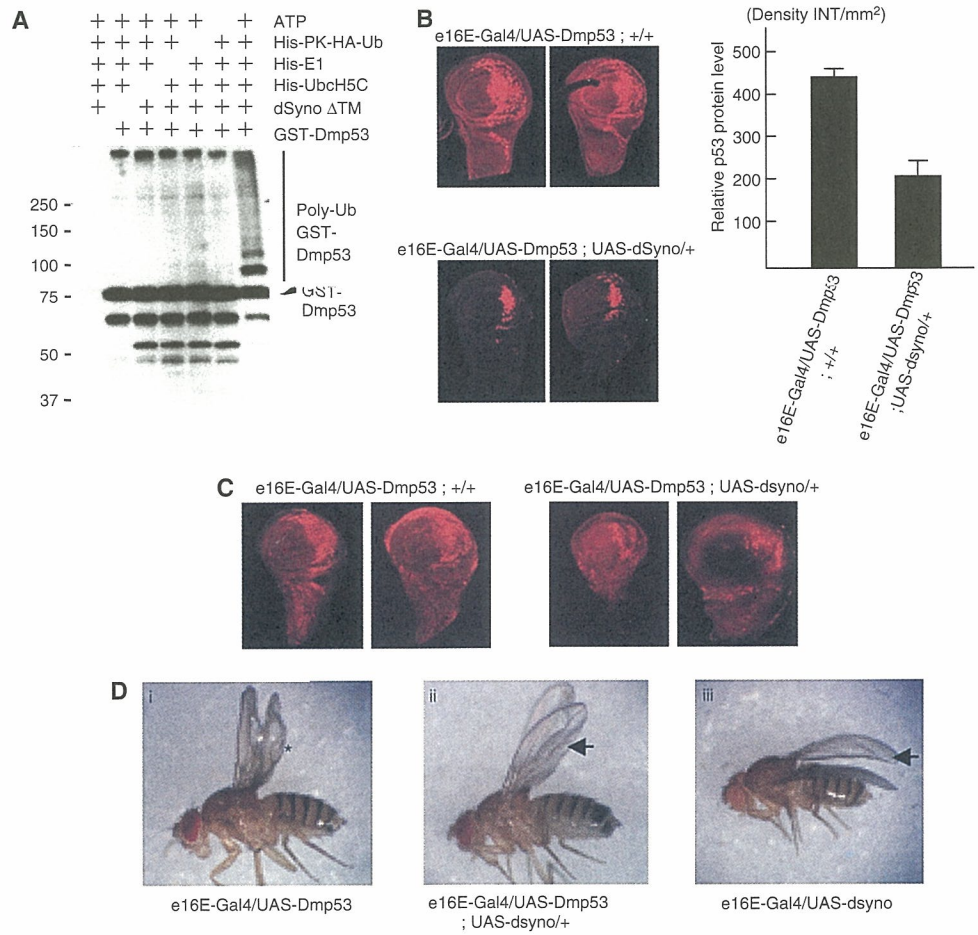

Figure 6 Synoviolin directly regulates p53-dependent apoptotic pathway in *Drosophila* fly. (**A**) Fly homolog of Synoviolin ubiquitinates fly homolog of p53 *in vitro*. GST-fusion *Drosophila melanogaster* p53 (Dmp53) was incubated with or without ATP, His-PK-HA-Ub, His-E1 (human), His-UbcH5C (human) and *Drosophila* Synoviolin (dSyno)ΔTM. Ubiquitinated proteins were probed with anti-HA antibody. (**B**) P53 protein level of wing discs was determined by immunostaining using anti-Dmp53 antibody (left). 2 representative pictures of each fly are shown. The fluorescence intensity of each 15 fly disc was quantified, and the net density level (Density INT/mm^2) was determined by subtracting the density level of the background area (anterior half of disc) from the measured level of the target area (posterior half of disc) (right). Data are mean±s.e.m. of $n=15$. (**C**) Apoptosis was examined by Acridine orange staining of wing disc. Overexpression of dSyno in the posterior half of the discs reduced Dmp53 overexpression-induced apoptosis. (**D**) Overexpression of dSyno suppressed the Dmp53-induced bubbled wing phenotype. The extent of wing bubble (*) in e16E-Gal4/UAS-Dmp53 flies varied with age, but the penetrance of bubbled wing phenotype was close to 100% (Supplementary Table 1). Overexpression of dSyno suppressed the Dmp53-induced bubbled wing phenotype, but dSyno-induced wrinkled phenotype at the posterior edge of wing was still observed (arrow).